NCS1 regulates Ca^{2+}-Dependent Focal Exocytosis of Golgi-derived Vesicles to Help Phagocytic uptake in Macrophages

Nimi Vashi[1], Syed Bilal Ahmad Andrabi[$,1], Swapnil Ghanwat[$,1], Mrutyunjay Suar[2] and Dhiraj Kumar*[,1]

[1]Cellular Immunology Group, International Centre for Genetic Engineering and Biotechnology, Aruna Asaf Ali Marg, New Delhi-110067, India

and

[2]School of Biotechnology, KIIT University, Bhubaneswar-751024, India

Running title: *Role of Golgi-derived vesicles in phagocytosis*

[$] Equal contribution

***Correspondence: dhiraj@icgeb.res.in**
Phone: +91-11-26742357
Fax: +91-11-26742316

Abstract

During phagocytic uptake by macrophages, role of Golgi apparatus or vesicles derived from it has never been established. Using fluorescently tagged Mannosidase-II, a marker for Golgi-derived vesicles, we show these vesicles are recruited during uptake of diverse targets including latex beads, *E. coli*, *Salmonella* Typhimurium and *Mycobacterium tuberculosis* in both human and mouse macrophages. The recruitment of Mannosidase-II vesicles occurred very early during phagocytosis, which was mediated by focal exocytosis. The focal movement of Mannosidase-II vesicles required Ca^{2+} from both extra- and intra-cellular sources apart from PI3Kinase, microtubules and dynamin-2. At the site of uptake voltage-gated Ca^{2+} channels help establish a Ca^{2+}-dependent local PIP3 gradient, which guide the focal movement. Mannosidase-II vesicles also contained Neuronal Calcium Sensor-1 (NCS1) and resembled secretory vesicles. Depleting NCS1 blocked the recruitment of Mannosidase-II vesicles and inhibited phagocytic uptake of diverse targets. We propose Golgi-derived vesicles provide membrane for phagosome biogenesis and are universally required for phagocytosis, the key innate defense function.

Introduction

Phagocytosis lies at the core of innate defense mechanisms in higher eukaryotes. The process of phagocytosis involves internalization of external particles including pathogens, cellular debris etc. into a specialized membrane bound organelle called phagosomes. The phagosome thus formed undergoes a series of fusion and fission events leading to acquisition of hydrolytic enzymes and microbicidal properties to mature into phago-lysosomes (Aderem and Underhill, 1999; Flannagan et al., 2012; Jutras and Desjardins, 2005).

It was perceived initially that the membrane for phagosomes could be solely derived from the plasma membrane (Cannon and Swanson, 1992). However in macrophages, the professional phagocytes, which can engulf objects bigger than their own size without significantly altering their function, there is no apparent decline in the membrane surface area following phagocytosis(Holevinsky and Nelson, 1998). Rather capacitance measurement experiments showed that a concomitant increase in the membrane surface area precedes resealing of the phagosome, suggesting supply of phagosome membrane from intracellular sources(Holevinsky and Nelson, 1998). Professional phagocytes are therefore expected to be under tremendous pressure to sustain the supply of the membrane so as to effectively phagocytize their targets. Consequently a variety of membrane bound organelles including the vesicles originating from recycling endosomes and lysosomes as well as ER were later shown to provide membrane for the nascent phagosome(Bajno et al., 2000; Gagnon et al., 2002; Tardieux et al., 1992).

Vesicle recruitment during phagocytosis involves exocytosis of vesicles in the vicinity of nascent phagosomes (Braun and Niedergang, 2006). Studies in the past have shown secretion of vesicular contents like lysosomal hydrolases and azurophil

72 granules during engulfment by macrophages and neutrophils respectively, thereby
73 coupling the process of phagocytosis with targeted exocytosis, a process also termed
74 as focal exocytosis (Bajno et al., 2000; Braun and Niedergang, 2006). Recycling
75 endosome marker VAMP3, a soluble N-ethylmaleimide-sensitive factor attachment
76 protein receptor proteins on vesicles (v-SNARE), was shown to accumulate at the
77 early phagosomes through focal exocytosis (Bajno et al., 2000). Moreover
78 Synaptotagmin V (SytV), a Ca^{2+} sensor on the recycling endosomes was shown to
79 regulate phagocytosis but not phagosome maturation, suggesting a key role of Ca^{2+} in
80 the regulation of vesicle exocytosis (Vinet et al., 2008). Similarly SytVII, a lysosome
81 resident Ca^{2+} sensor was reported to regulate delivery of lysosome membrane to the
82 nascent phagosomes (Czibener et al., 2006). Interestingly, SytVII was also shown to
83 regulate Ca^{2+} dependent exocytosis of lysosomes during plasma membrane repair
84 (Reddy et al., 2001). Recently TRPML1, a key Ca^{2+} channel in the lysosomes was
85 shown to regulate focal exocytosis during phagocytosis of large particles (Samie et
86 al., 2013). Phosphoinositide3kinase (PI3K) is yet another key regulator of
87 phagocytosis, and is believed to help pseudopod extension around the particles during
88 phagocytosis (Cox et al., 1999). However, inhibition of PI3K by wortmannin may not
89 limit membrane availability for phagocytosis (Cox et al., 1999). There are some
90 reports however suggesting the role of PI3K in recruiting the membranes from
91 intracellular sources (Underhill and Ozinsky, 2002). Yet another study revealed
92 recruitment of endoplasmic reticulum (ER) at the site of phagocytosis to provide
93 membrane for the newly formed phagosomes, a process that was regulated by the ER
94 resident SNARE protein ERS24 (Gagnon et al., 2002; Jutras and Desjardins, 2005).
95 Intriguingly, despite being intricately involved with the recycling endocytic network
96 and as one of the major sources of vesicles destined to the plasma membrane like

secretory vesicles, involvement of Golgi Apparatus (GA) or vesicles derived from GA in the process of phagocytosis has been ruled out (Becker et al., 2005). However in an interesting observation, fragmentation and reorganization of GA was reported during a process of frustrated phagocytosis (Bainton et al., 1989). Interestingly majority of the reports that conclude no direct involvement of GA during phagocytic uptake relied on the experiments that were limited to Fcγ-Receptor mediated phagocytosis (Beemiller et al., 2006; Braun et al., 2007; Zhang et al., 1998). Here we studied the role of vesicles derived from the GA during phagocytic uptake. Mannosidase-II, a medial and trans-Golgi marker was also detected within secretory granules and at the surface of certain cell types like enterocytes, pancreatic acinar cells and goblet cells (Velasco et al., 1993). Later, using Mannosidase-II as the marker of Golgi-derived vesicles its recruitment to cell surface was used to track the role of these vesicles during plasma membrane repair in mouse bone marrow derived primary macrophages (Divangahi et al., 2009; Velasco et al., 1993). Here we show, Mannosidase-II containing Golgi-derived vesicles are recruited during phagocytosis of a variety of targets including inert particles (latex beads), non-pathogenic bacteria (*E. coli*) and pathogenic bacteria (*Salmonella* Typhimurium and *Mycobacterium tuberculosis*) in mouse (RAW264.7 and BMDMs) and human (THP-1 and U937) macrophages. The recruitment of Mannosidase-II vesicles at the site of phagocytosis occurred through the process of focal exocytosis. This process was dependent on voltage-gated Ca^{2+} channels that helped establish a Ca^{2+} dependent PIP3 gradient for uptake. Mechanistically, TGN and secretory vesicle resident protein NCS1 sensed and triggered the movement of vesicles to help phagosome biogenesis.

121 ## Results

122 **α-Mannosidase-II (MAN2A) localizes to Golgi Apparatus (GA) and Golgi**
123 **derived vesicles**

124 To confirm the localization of Mannosidase-II to GA in our experimental set-up, we
125 nucleofected THP-1 human macrophages and RAW264.7 mouse macrophages with a
126 mCherry-tagged Mannosidase-II construct [mCherry-MannII-N-10 (mCherry-
127 MAN2A), Addgene plasmid # 55074] and visualized the cells under Nikon A1R
128 confocal microscope (see methods). Expression of Mannosidase-II in these cells
129 distinctly labeled the GA as shown in figure 1A. We also immuno-stained
130 Mannosidase-II using specific antibody, which labeled the GA (Fig. 1B). Treatment
131 of mCherry-MAN2A expressing cells with Brefeldin A, the classical inhibitor of
132 Golgi function, resulted in the disruption and fragmentation of the GA structure (Fig
133 1C). In both transfected as well as antibody stained cells, in addition to the main GA
134 we could also observe several smaller punctate structures, representing the Golgi-
135 derived vesicles (Fig. 1A and B). In U937 cells stably expressing mRuby-tagged
136 Beta-1,4-Galactosyltransferase (B4GALT1-mRuby), a mid-Golgi resident enzyme, no
137 such vesicle like structures could be seen (Fig. 1D), Mannosidase-II however co-
138 localized with B4GALT1-mRuby (Fig. 1D). These results confirmed that the
139 Mannosidase-II construct used in this study labeled GA and Golgi-derived vesicles.

140 **Mannosidase-II is recruited at the site of phagocytic uptake**

141 RAW264.7 cells transfected with mCherry tagged Mannosidase-II were incubated
142 with mouse-IgG coated latex beads (see methods) that were either unstained or
143 stained with anti-mouse IgG-Alexa488. At 30 minutes and one-hour post-addition of
144 beads to the macrophages, cells were fixed and visualized under the microscope. We
145 observed the recruitment of Mannosidase-II to the sites where latex beads were

146 phagocytosed, forming ring like structure around the beads at many instances (Fig.
147 2A and Fig. S1A). Overall intensity of Mannosidase-II at the bead surface had a
148 median of ~900 at 30 minutes and ~1500 arbitrary units (A.U.) at 1 hour as
149 determined using the 3-D module tool in Imaris 7.2 (see methods, Fig 2A). To check
150 whether Mannosidase-II recruitment during phagocytosis was a general phenomenon
151 we also monitored uptake of non-pathogenic bacterium *E. coli* and pathogenic
152 bacteria *Salmonella* Typhimurium. In both the cases, we could see Mannosidase-II
153 recruited at very early stages of phagocytosis. In the case of *E. coli,* nearly 60% of the
154 bacteria at the site of entry showed Mannosidase-II recruitment at 15 and 30 minutes
155 post-infection while nearly 30% of *Salmonella* containing phagosomes showed
156 Mannosidase-II recruitment at 5 and 10 minutes (Fig 2B). In the case of yet another
157 pathogenic bacteria *Mycobacterium tuberculosis* strain H37Rv, Mannosidase-II was
158 recruited at 30-40% phagosomes at the time of entry (Fig. 2C). Recruitment of
159 Mannosidase-II at the early phagosomes in case of H37Rv was also verified by
160 immuno-staining against Mannosidase-II (Fig. S1B). To confirm that the
161 Mannosidase-II positive phagosomes indeed represented early stages of phagosomes,
162 we immuno-stained the mCherry-MAN2A expressing cells, that were either incubated
163 with mouse-IgG coated latex beads or infected with *Mtb*, with anti-transferrin
164 receptor (TfR) antibody. We observed significant overlap between recruited
165 Mannosidase-II and TfR around the internalized beads and *Mtb* (Fig. 2D and 2E). TfR
166 recruitment around phagocytized beads showed saturating levels with median of
167 around 4095 A.U., much higher than the intensity distribution of Mannosidase-II
168 (~1000 A.U., Fig. 2D). In case of *Mtb* too, TfR showed relatively higher co-
169 localization with the phagosomes (~40-60%) compared to Mannosidase-II (30-50%,
170 Fig. 2E). Expectedly, TfR on *Mtb* phagosomes declined rapidly from one-hour post

171 infection to two hours post infection (Fig. 2E). To further establish that the membrane
172 recruitment of Mannosidase-II during phagocytosis was an early event, we took U937
173 cells that stably expressed EGFP fused with a plasma membrane targeting sequence
174 from Neuromodulin (Liu et al., 1991). We nucleofected these cells with mCherry-
175 MAN2A followed by incubation with the latex beads. As shown in figure 2F,
176 Mannosidase-II was recruited at the site of phagocytosis where it mostly localized to
177 the cytosolic face of the newly forming phagosome while the latex beads were still
178 getting internalized. We also verified the recruitment of Mannosidase-II in mouse
179 bone marrow derived macrophages (BMDMs) during phagocytic uptake of *E. coli*,
180 thus ensuring that it was not a phenomenon restricted to only cell-lines (Fig. S1C).

181 **Characterization of early phagosomes reveals direct involvement of secretory**
182 **vesicles derived from the GA in the phagosome biogenesis**

183 As shown above and by others (Divangahi et al., 2009; Velasco et al., 1993),
184 Mannosidase-II marks both GA and Golgi-derived vesicles. In most of the fields
185 observed in the previous sections, we could see Mannosidase-II organized into a
186 separate Golgi structure, underscoring the fact that the phagosome associated
187 Mannosidase-II were derived from the recruitment of Golgi-derived vesicles at the
188 site of infection. To further confirm the selective enrichment of Mannosidase-II at the
189 nascent phagosomes, we purified latex beads phagosomes using sucrose density
190 gradient ultra-centrifugation from macrophages within 1 hour of uptake (Fig. 3A).
191 The phagosome preparation showed presence of expected early phagosome markers
192 like TfR and RAB5 (Fig. 3B). They also showed presence of previously reported
193 markers like VAMP3 from recycling endosomes and Calnexin from ER (Fig. 3B). At
194 the same time, the phagosome preparation was devoid of any mitochondrial, nuclear
195 or cytosolic contamination (Fig. 3B). In agreement with the microscopy data,

196 phagosomes also showed presence of Mannosidase-II, the marker for Golgi-derived
197 vesicles (Fig. 3B). In addition, we could also score the presence of another Golgi-
198 derived secretory vesicles marker NCS1 in the phagosomes (Fig. 3B). We verified
199 that there was no GA contamination in the preparation as the phagosomes were
200 devoid of B4GALT1 (Fig. 3B).
201 Trafficking of vesicles in the cells is regulated by a large number of proteins
202 including small GTPases like RABs, ADP-Ribosylation factors (ARFs) and SNAREs
203 (Chen and Scheller, 2001; Gillingham and Munro, 2007; Stenmark, 2009). In order to
204 understand which RABs, SNAREs or ARFs could be involved in the recruitment of
205 Mannosidase-II vesicles at the phagosomes we performed mass-spectrometry of the
206 purified latex beads phagosome preparations, specifically to identify molecules below
207 25kDa molecular weight (Fig. S2, see methods). We were able to identify about 290
208 proteins from this preparation, all of them below 25kDa molecular weight
209 (Supplementary table S1). We performed a gene ontology analysis on these proteins
210 using Amigo2.0 database to specifically see enrichment of eleven classes including
211 ER, GA, secretory vesicles, recycling endosomes, endocytic vesicles,
212 neurotransmitter release, TGN, vesicle mediated transport, phagocytosis/engulfment,
213 exocytosis and endosomal transport (Fig. 3C, Supplementary table S2). A large
214 number of proteins belonging to ER were found in the phagosomes (Fig. 3C). The
215 phagosome mass spectrometry data revealed presence of 17 different RABs, 5 out of
216 6 known ARFs and four VAMPs. Many of these proteins are involved with Golgi
217 apparatus, exocytosis, secretory vesicles and neurotransmitter release (Fig. 3C).
218 VAMP2 gets enriched in the secretory vesicles that are released from the GA and
219 targeted to the membranes (Faurschou and Borregaard, 2003). It also helps in the
220 release of neurotransmitters by regulating the exocytosis of secretory vesicles (Shen et

221 al., 2015). Presence of a large variety of proteins that could regulate vesicle
222 trafficking on the early phagosomes could potentially mean a complex interplay of
223 different vesicle trafficking pathways in the process of phagosome biogenesis. Since
224 the role of vesicles derived from recycling endosomes and involvement of ER was
225 already established during phagosome biogenesis, presence of markers associated
226 with vesicles derived from the GA reconfirmed the utility of this organelle as an
227 additional source of membranes for phagosome biogenesis.

228 **Mannosidase-II positive Golgi-derived vesicles are recruited at the phagosomes**
229 **through focal exocytosis**

230 We next wanted to understand how Mannosidase-II vesicle recruitment was regulated
231 during phagocytosis. It was previously reported that Mannosidase-II positive Golgi-
232 derived vesicles get recruited at the site of membrane damage during repair
233 (Divangahi et al., 2009). It is also well established that vesicular movement during
234 membrane repair occurs through focal exocytosis (Reddy et al., 2001). To verify the
235 recruitment of Mannosidase-II during membrane repair, we treated RAW264.7
236 macrophages expressing mCherry-MAN2A with detergent for 15 minutes to cause
237 membrane damage. The cells were then followed live for next 2-3 hours to assess
238 recruitment of Mannosidase-II at the damaged site. We could observe formation of
239 membrane lesion upon detergent treatment and subsequent recruitment of
240 Mannosidase-II that eventually sealed the lesion (Fig. S3) thereby highlighting the
241 targeted exocytic movement of Mannosidase-II vesicles.

242 One of the key regulators of focal exocytosis, specifically for post-Golgi transport
243 vesicles towards the plasma membrane, is dynamin (Kreitzer et al., 2000). Dynamins
244 are the member of large GTPase family and dynamin-2 is the ubiquitously expressed
245 isoform while dynamin-1 is mostly neuronal (Henley and McNiven, 1996; Warnock

246 et al., 1997). Their involvement in budding of transport vesicles from the Golgi is also
247 well documented along with their role in regulating focal exocytosis (Praefcke and
248 McMahon, 2004; Samie et al., 2013). In mCherry-MAN2A expressing RAW264.7
249 cells, we observed significant overlap of Mannosidase-II with dynamin-2 on the
250 phagosomes containing either latex beads or *Mtb* (Fig. 4A and 4B). Again as in the
251 case of TfR, dynamin-2 recruitment on the nascent phagosomes was relatively higher
252 than Mannosidase-II recruitment for both latex beads and *Mtb* (Fig. 4A and 4B).
253 Presence of dynamin-2 at the phagosomes was consistent with previous reports,
254 which showed their recruitment at early phagosomes during phagocytosis (Gold et al.,
255 1999).
256 We next inhibited dynamin-2 by dynasore treatment for varying period of time and
257 observed its effect on Mannosidase-II recruitment and phagocytosis. In the case of
258 latex beads, four hours of pre-treatment with dynasore (at 40 and 80μM) resulted in a
259 significant inhibition in the recruitment of Mannosidase-II at the phagosomes (Fig.
260 4C). It also markedly reduced the phagocytosis of latex beads (Fig. 4D). Dynasore
261 treatment also inhibited uptake of *Mtb* in THP-1 macrophages (Fig. S4A). There was
262 noticeable decline in the recruitment of Mannosidase-II at the *Mtb* phagosomes (Fig.
263 S4B). Dynamin assisted movement of vesicles also require microtubules (Kreitzer et
264 al., 2000). Inhibition of microtubules by nocodazole treatment resulted in a transient
265 decline in the uptake of *Mtb* and latex beads (Fig. S4C and D). Further, nocodazole
266 treatment resulted in a marked decline in the recruitment of Mannosidase-II to the
267 phagosomes containing latex beads and *Mtb* (Fig. S4E and F). These results
268 established that the Mannosidase-II positive Golgi-derived vesicles were recruited at
269 the phagosomes through focal exocytosis and were assisted by dynamins.

270 **Golgi-derived vesicles co-operate with the vesicles derived from the recycling**
271 **endosomes during phagocytosis**
272 Recruitment of vesicles from endocytic origin (VAMP3 positive) and lysosomal
273 origin (LAMP1 positive) during phagocytosis has been reported earlier (Bajno et al.,
274 2000; Czibener et al., 2006). We also observed presence of VAMP3 on the early latex
275 beads phagosomes as shown above (Fig. 3B). This finding was reconfirmed in
276 mCherry-MAN2A expressing RAW264.7 cells, where both latex beads and *Mtb* very
277 early during phagocytosis (30 minutes and 1 hour for beads; 1 hour and 2 hours for
278 *Mtb*) showed very high recruitment of and co-localization with VAMP-3 (Fig. 4E and
279 F). In case of *Mtb*, more than 90% of the Mannosidase-II positive phagosomes were
280 also positive for VAMP-3 (Fig. 4F). Overall, VAMP-3 recruitment was much higher
281 compared to Mannosidase-II recruitment at the site of phagocytosis (Fig. 4E and F).
282 Thus spatially and temporally, Mannosidase-II recruitment at the phagosomes was
283 strikingly similar to VAMP3 recruitment. Moreover similar to the case of Golgi-
284 derived vesicles here, the recruitment of VAMP-3 positive vesicles from the recycling
285 endosomes is also dependent on focal exocytosis (Bajno et al., 2000). Thus it is very
286 likely that vesicles from different origins co-operate in aiding the biogenesis of
287 phagosomes.
288 **Phosohatidylinositol3Kinase (PI3K) is required for Mannosidase-II recruitment**
289 **at the nascent phagosomes and phagocytosis**
290 The role of PI3K in regulating phagocytosis is well known where its function is
291 believed to be mostly required for pseudopod extension around the cargo during
292 phagocytosis (Cox et al., 1999). We wanted to test whether some of the effects of
293 PI3K on phagocytosis were due to its involvement in the recruitment of Mannosidase-
294 II vesicles for phagocytosis. Inhibition of PI3K by wortmannin led to nearly 80%

295 decline in the uptake of latex beads at 30 and 60 minutes (Fig. 5A). In case of *Mtb*,
296 the decline in uptake was ~85% at 1 and 2 hours post-infection and 70% at 4 hours
297 post-infection (Fig. 5B). In the case of *Mtb* we assayed multiple doses of wortmannin
298 and three different MOIs (Fig. S5A). The effect of wortmannin on the uptake of *Mtb*
299 was dependent on the inhibitor concentration however independent of the MOIs used
300 (Fig. S5A). Wortmannin was equally effective in inhibiting the phagocytic uptake of
301 *Salmonella* Typhimurium in THP-1 macrophages (Fig. S5B). Curiously, PI3K
302 inhibition also resulted in a marked decrease in the recruitment of Mannosidase-II at
303 the nascent phagosomes (Fig. 5C and D). Thus at least to some extent, it seems the
304 effect of inhibition of PI3K on phagocytosis may be due to a reduced recruitment of
305 Mannosidase-II positive Golgi-derived vesicles at the phagosomes. Similar effect of
306 PI3K inhibition on the membrane recruitment for the newly forming phagosomes has
307 been discussed previously (Underhill and Ozinsky, 2002).

308 **Extracellular Calcium (Ca^{2+}) is needed for phagocytosis and focal exocytosis of**
309 **Golgi-derived vesicles at the site of phagocytosis**

310 We next wanted to understand the immediate early mediators of focal exocytosis
311 during phagocytosis. Focal exocytosis of vesicles derived from the recycling
312 endosomes as well as lysosomes depends on the functioning of key Ca^{2+} sensors in
313 these compartments (Czibener et al., 2006; Samie et al., 2013; Vinet et al., 2008). It
314 was therefore imperative to test the role of Ca^{2+} in the focal movement of Golgi-
315 derived vesicles. Release of Ca^{2+} from intracellular stores is one of the key signaling
316 events during the course of phagocytosis and downstream maturation of the
317 phagosomes (Koul et al., 2004). Expectedly, phagocytosis of both latex beads and
318 H37Rv in THP-1 macrophages was severely hampered in the presence of TMB-8
319 (Fig. 5E and F), an inhibitor of the IP3 receptor that serves as the Ca^{2+} release channel

320 from intracellular stores like ER upon binding with IP3 (Singh et al., 2005).
321 Intriguingly, presence of Ca^{2+} chelator EGTA in the extracellular media also inhibited
322 phagocytic uptake of both latex beads and H37Rv in THP-1 macrophages (Fig. 5E
323 and F) thereby suggesting the involvement of extracellular Ca^{2+} in the phagocytic
324 uptake. However it could simply imply the effect of capacitative Ca^{2+} influx, which
325 typically requires the CRAC channels and happens immediately after the intracellular
326 stores are exhausted of Ca^{2+} (Singh et al., 2005). Treatment with both TMB-8 and
327 EGTA had additive effect on the uptake of latex beads but not on the uptake of *Mtb*
328 by THP-1 macrophages (Fig. 5E and F). We also noted a much more pronounced and
329 sustained effect of TMB-8 and EGTA+TMB8 (~70% and ~85% inhibition
330 respectively, Fig. 5E) on the uptake of latex beads as against that of *Mtb* (~25% and
331 ~45% inhibition respectively, Fig. 5F). As observed in the case of wortmannin
332 treatment, inhibition of Ca^{2+} signaling also resulted in a marked decline in the
333 recruitment of Mannosidase-II at the nascent phagosomes (Fig. 5C and D).

334 **Entry of extracellular Ca^{2+} through voltage-gated Ca^{2+} channels helps create the**
335 **foci for the recruitment of vesicles during phagocytosis**

336 The role and mechanism of recruitment of extracellular Ca^{2+} during phagocytosis is
337 limited to the capacitative influx (Lee et al., 2003) or through passive accumulation of
338 Ca^{2+} in the phagosomes during phagocytosis (Lundqvist-Gustafsson et al., 2000). An
339 increase in the local Ca^{2+} concentration around phagosomes has been reported to
340 facilitate phagocytosis (Stendahl et al., 1994). Interestingly, the role of extracellular
341 Ca^{2+} during membrane repair process and focal exocytosis of vesicles to the damaged
342 site has been extensively reported (Miyake and McNeil, 1995; Steinhardt et al., 1994;
343 Togo et al., 1999). Similarly during neurotransmitter release in the neuronal cells,
344 activation of voltage-gated Ca^{2+} channels during action potential helps focal

345 exocytosis of secretory vesicles (Sudhof, 2012). We hypothesized that one of the
346 earliest signals during phagocytic uptake could consist of Ca^{2+} entry into the cells
347 through the voltage-gated Ca^{2+} channel. In THP-1 macrophages treated with
348 loperamide hydrochloride or amlodipine besylate (inhibitors of L/P-type and L –type
349 voltage gated Ca^{2+} channels respectively) (Church et al., 1994; Kochegarov, 2003),
350 phagocytosis of *E. coli* declined considerably (Fig. 6A). These treatments were also
351 effective against phagocytosis of *Mtb* and latex beads in THP-1 macrophages (Fig.
352 S6A and B). Treatment with any of these two inhibitors also blocked Mannosidase-II
353 recruitment at the nascent phagosomes during uptake of latex beads in THP-1
354 macrophages (Fig. 6B). Thus voltage-gated channel seems to play an important role
355 during phagocytosis of diverse targets.
356 We next wanted to understand whether extracellular Ca^{2+} helped decide the foci for
357 the recruitment of Golgi-derived vesicles during phagosome formation (Sudhof,
358 2012). We investigated the accumulation of PIP3 at the site of engulfment. Inhibition
359 of PIP3 by wortmannin treatment abrogates the uptake as observed in this study (Fig.
360 5) as well as reported earlier (Cox et al., 1999). PIP3 is known to interact with the
361 Pleckstrin Homology (PH) domain of proteins. In cells expressing AKT-PH domain
362 fused with mCherry (AKT-PH-mCherry), at 5 minutes post-addition of *E. coli*, we
363 observed, expectedly, a significant accumulation of PIP3 at the site of bacterial entry
364 (Fig. 6C). Also there was a gradual decline in the PIP3 levels as we move further into
365 the cells from the site of phagocytosis (Fig. 6C). However in cells pre-treated with the
366 Ca^{2+} chelator (EGTA, 3mM), the selective accumulation of PIP3 at the site of
367 phagocytosis was lost (Fig. 6C) and PIP3 was almost uniformly distributed across the
368 cell irrespective of the site of engagement with the bacteria (Fig. 6C). Surprisingly,
369 similar effect on PIP3 distribution was observed when these cells were pre-treated

370 with either loperamide or amlodipine (Fig. 6C). In both these cases, the distribution of
371 PIP3 in the cells was not influenced by the site of engagement with the bacteria (Fig.
372 6C). In cells treated with the PI3K inhibitor wortmannin, AKT-PH-mCherry was as
373 expected, more uniformly distributed (Fig. 6C). Quantitatively, it was evident from
374 the signal intensity plots (see methods) in figure 6D, that a gradient of PIP3 is
375 established during phagocytosis, with the highest concenration at the site of entry.
376 Moreover since blocking the entry of extracellular Ca^{2+} either through chelators or
377 inhibitors of voltage gated channels resulted in a loss of PIP3 gradient in a similar
378 fashion as in the case of wortmannin treatment, it was evident that the formation of
379 PIP3 gradient was dependent on Ca^{2+}, more liekly on the entry of Ca^{2+} from
380 extracellular milieu through the voltage-gated Ca^{2+} channels (Fig. 6D). Together these
381 results imply that the extracellular Ca^{2+}, entering through a voltage-gated Ca^{2+}
382 channel helps forming the foci for the recruitment of PI3K and initiate the signaling
383 cascade for phagocytic uptake in the macrophages.

384 **Mannosidase-II positive early phagosomes are also NCS1 positive**

385 Having established the role of Ca^{2+} in regulating the movement of Mannosidase-II
386 vesicles during phagocytosis, we next wanted to understand how the focal movement
387 of Golgi-derived vesicles is triggered in phagocytosing macrophages. NCS1 is an EF-
388 hand motif containing protein, originally believed to exclusively express in the
389 neuronal cells (Haynes et al., 2005). Subsequently it was shown to get expressed in a
390 variety of cell lines as TGN resident Ca^{2+} interacting protein (Haynes et al., 2005).
391 NCS1 was reported to be involved in the recruitment of Golgi-derived vesicles during
392 plasma membrane repair in macrophages and was integral to these vesicles (Behar et
393 al., 2010; Divangahi et al., 2009). In cells expressing mCherry-MAN2A we stained
394 for NCS1 during uptake of latex beads or Mtb. In both the cases, NCS1 co-localized

395 with the cargo (Fig. 7A, Fig. S7A). In the case of Mtb, nearly all Mtb containing
396 phagosomes were also positive for NCS1 whereas some NCS1 positive phagosomes
397 did not contain Mannosidase-II (Fig. 7A). Similarly for beads, NCS1 intensity was
398 much higher compared to Mannosidase-II intensity (Fig. 7B). Moreover, we observed
399 NCS1 to co-localize with Mannosidase-II in vesicles that were not part of the
400 phagosome (Fig. S7B), corroborating with the fact that both Mannosidase-II and
401 NCS1 are components of the GA secretory vesicles derived from the GA (Behar et
402 al., 2010; Divangahi et al., 2009).

403 **Depleting Neuronal Calcium Sensor 1 (NCS1) inhibits focal exocytosis of**
404 **MAN2A vesicle during phagocytosis**

405 To test whether Ca^{2+} dependent trigger of vesicular trafficking relied on the ability of
406 NCS1 activation upon Ca^{2+} binding, we compared the recruitment of Mannosidase-II
407 at the nascent phagosome during phagocytosis of *E. coli* in THP-1 macrophages that
408 were either treated with scrambled siRNA control or NCS1 specific siRNA (Fig.
409 S7C). Knocking down NCS1 resulted in more than 50% decline in the recruitment of
410 Mannosidase-II at the early *E. coli* phagosomes (Fig. 7C). Expectedly, knockdown of
411 NCS1 in THP-1 macrophages resulted in a marked decline in the uptake of latex
412 beads, *E. coli*, *Salmonella* and *Mtb* (Fig. 7D). True to all other treatments, which
413 inhibited the phagocytic uptake, NCS1 siRNA knockdown also had both quantitative
414 and kinetic effects on the uptake of all of the targets except in *Salmonella* where the
415 effects were persistent (Fig. 7D). Thus uptake in case of latex beads was ~35, 60 and
416 85% of the control in the siRNA treated sets at 30 minutes, 1 hours and 2 hours
417 respectively (Fig. 7D). For *E. coli* these numbers were 8, 10 and 22% of control at 5,
418 15 and 30 minutes (Fig. 7D). In case of *Salmonella*, uptake was about 65% of the
419 control set at 15 and 30 minutes while in case of *Mtb*, the relative uptake in the NCS

420 knockdown cells was 40, 45 and 55% of control at 1 hour, 2 hours and 4 hours

421 respectively (Fig. 7D).

422

Discussions

Professional phagocytes like macrophages require continuous supply of membrane in order to form phagosomes around the phagocytosed particles (Vicker, 1977). It is now understood that cellular compartments like recycling endosomes, lysosomes and ER could supply membrane for the nascent phagosomes (Bajno et al., 2000; Tardieux et al., 1992), (Gagnon et al., 2002). Adding to the existing pool of membrane sources available for phagosome formation, in this study we show recruitment of Golgi-derived vesicles at the site of phagocytosis in macrophages. However unlike previous reports, where the studies were mostly restricted to either latex beads or select organism, we show here a more universal requirement of the Golgi-derived vesicles during phagocytosis by macrophages using inert particles, non-pathogenic bacteria and two different pathogenic bacterial species as the cargo. It is important to note here that GA serves as the origin for most vesicles in the cell, including recycling endosomes, endocytic machinery and vesicles destined to the plasma membrane for exocytosis (Bonifacino and Glick, 2004). Bacterial pathogens once inside the host cells further subvert the membrane trafficking pathways to ensure prolonged survival and escape from innate defense mechanisms(Alix et al., 2011). Interestingly GA serves as the hub for trafficking inside the cells (Gillingham and Munro, 2016). It therefore may make strong sense that GA gets involved and alerted of incoming pathogen while the cell has just started to engulf it. This line of investigation seems extremely fascinating at present as it may open a new understanding in the functioning of innate immune system.

Role of Golgi-derived vesicles in supplying the membrane at plasma membrane is well known at least in one context - the membrane repair pathway (Divangahi et al., 2009). Using Mannosidase-II as specific marker for Golgi-derived vesicles they

448 showed participation of GA and lysosomes in the repair process through targeted
449 exocytosis (Divangahi et al., 2009). The movement of vesicles during phagocytosis
450 from the recycling endosomes and lysosomes was also reported to follow a similar
451 targeted exocytosis where vesicles are directed towards the phagocytic cup (Bajno et
452 al., 2000; Niedergang and Chavrier, 2004; Samie et al., 2013). Interestingly more than
453 90% of Mannosidase-II positive phagosomes at the site of entry were also found to be
454 positive for VAMP-3 and dynamin-2. While VAMP-3 gets recruited through focal
455 exocytosis, dynamin-2 is known to regulate post-Golgi transport of vesicles and
456 facilitate focal exocytosis (Samie et al., 2013). Dynamins have earlier been implicated
457 in regulating the focal exocytosis in phagocytosing macrophages (Di et al., 2003;
458 Gold et al., 1999; Samie et al., 2013). Inhibition of dynamins by dynasore treatment
459 resulted in a reduced phagocytic uptake, which may simply occur due to inhibition of
460 dynamin-mediated scission of phagosomes from the membrane (Jones et al., 1998).
461 However dynasore treatment also resulted in reduced Mannosidase-II recruitment at
462 the nascent phagosomes, implying the involvement of roles dynamin plays in vesicle
463 budding and their focal movement towards the site of uptake. High co-localization of
464 Mannosidase-II with TfR further emphasized very early recruitment of Golgi-derived
465 vesicles. Yet another instance where vesicle exocytosis from Golgi has been
466 extensively studied is in the context of neurotransmitter release, which shows
467 remarkable similarity with the focal exocytosis during membrane repair. Thus it is
468 intriguing to witness the brilliance of cellular economy, where a common mechanism
469 could be utilized to address three entirely independent cellular requirements.
470 Next to understand how target recognition at the cell surface for phagocytic uptake
471 could trigger GA to elicit the movement of the vesicles, we took cues from membrane
472 repair pathway where the damage is typically sensed via entry of extracellular Ca^{2+}

473 into the cells (Miyake and McNeil, 1995; Steinhardt et al., 1994). We indeed observed
474 inhibiting either extracellular Ca^{2+} or the release of Ca^{2+} from intracellular stores
475 resulted in a loss of phagocytic function in the macrophages. The possibility of a
476 membrane breach during phagocytic uptake in macrophages has never been
477 discussed. Thus most plausible source for the entry of extracellular Ca^{2+} was some
478 membrane channels, which are classically involved at a similar step during
479 neurotransmitter release(Augustine, 2001; Sudhof, 2012). Experiments with
480 loperamide and amlodipine strongly support a critical involvement of voltage-gated
481 Ca^{2+} channel in the extracellular Ca^{2+} entry thereby facilitating phagocytosis.
482 Incidentally the role of voltage-gated channel in regulating podosome formation in the
483 macrophages was recently shown (Carrithers et al., 2009). Yet another channel
484 TRPV2 was recently shown to be important for phagocytosis in macrophages and its
485 absence resulted in loss of Ca^{2+} influx from the extracellular milieu and abrogated
486 phagocytic uptake (Link et al., 2010). Curiously macrophages lacking TRPV2 were
487 also defective in chemoattractant-evoked motility (Link et al., 2010). It may not be
488 unusual to assume that some of the inhibitory effects shown in this study were most
489 likely due to inhibition of TRPV channels at the plasma membrane. Therefore it
490 seems macrophage membrane depolarization could be a more general mechanism of
491 cellular functioning including phagocytosis, adherence and motility.
492 Phagocytosis was also dependent on the release of Ca^{2+} from intracellular stores, as
493 TMB8 treatment inhibited phagocytosis. A combination of EGTA and TMB8 had
494 more dramatic effects on phagocytosis, which also showed some sort of selectivity in
495 terms of the cargo. Thus, for latex beads, blocking both intra- and extra-cellular cargo
496 abolished their uptake by the macrophages, however in case of bacteria, the block in
497 uptake was more kinetic in nature. It strongly supports the possibility that Ca^{2+} may

498 be extremely critical for the uptake of cargos where cognate receptors are not
499 known/available thereby rely a lot on the membrane depolarization and associated
500 Ca^{2+} entry. The graded importance of Ca^{2+} during phagocytosis of diverse targets
501 needs further exploration for better understanding. Inhibition of Ca^{2+} also resulted in
502 reduced Mannosidase-II recruitment at the phagosomes.
503 The role of PI3Kinase in phagocytosis is well known, which supposedly helps
504 pseudopod extension while engulfing the target (Cox et al., 1999). However, it has
505 also been shown that inhibition of PI3Kinase may limit the membrane availability
506 (Underhill and Ozinsky, 2002). We indeed observed uptake of *Mtb*, *Salmonella* or
507 latex beads by macrophages were severely compromised in the presence of
508 wortmannin. *Salmonella* entry is known to occur via either macropinocytosis or
509 phagocytosis, however the former is insensitive to PI3Kinase inhibition(Drecktrah et
510 al., 2006). Thus the strains used in this study taken up by the macrophages thorugh
511 phagocytosis. Interestingly vesicle recruitment has also been reported to be important
512 for membrane ruffle formation, which helps in Salmonella macropinocytosis (Dai et
513 al., 2007). We also noted significantly reduced recruitment of Mannosidase-II vesicles
514 at the nascent phagosomes in the presence of wortmannin. Thus recruitment of Golgi-
515 derived vesicles at the nascent phagosomes indeed required PIP3. Experiments with
516 AKT-PH-mCherry clearly support the establishment of PIP3 gradient during
517 phagocytosis. Selective PIP3 enrichment has previously been shown regulating
518 cellular polarity, chemotaxis and pseudopod extension (Cox et al., 1999; Funamoto et
519 al., 2002; Ridley et al., 2003). The most dramatic observation was however the use of
520 voltage-gated Ca^{2+} channels by macrophages to set the foci for PIP3 accumulation,
521 which eventually results in all the downstream signaling and recruitments.
522 Interestingly, dynamins have conserved PH-domain at their C-terminal, making them

523 responsive to the PIP3 levels. It has been shown that mutations in the PH domain of
524 dynamin could result in severe defects in its key functioning like post-Golgi transport
525 and endocytosis (Achiriloaie et al., 1999; Zuchner et al., 2005). Thus PI3K and
526 dynamins seem to work together for the focal recruitment of Golgi-derived vesicles
527 during phagosome biogenesis.
528 The Ca^{2+} sensing function in the GA is attributed to the resident molecule NCS1,
529 which was initially discovered in the neuronal cells regulating the synaptic
530 transmission (Haynes et al., 2005). NCS1 was also shown as part of the secretory
531 vesicles (Scalettar et al., 2002). In macrophages, ablation of NCS1 resulted in a block
532 in the membrane-resealing pathway (Divangahi et al., 2009). We therefore
533 hypothesized; NCS1 could also serve as the Ca^{2+} sensor in Golgi apparatus for
534 triggering the exodus of the vesicles during phagocytosis. Interestingly, NCS1
535 knockdown not only reduced the phagocytic function of macrophages, there was also
536 significantly lower recruitment of Mannosidase-II at the phagosomes.
537 The results form purified latex beads phagosomes supported the overall observation in
538 this study that phagocytic uptake is a complex process and involves several players.
539 We deliberately focused on the molecules below 25kDa cut-off to make sure
540 enrichment of three key classes of molecules including RABs (~25 kDa), ARFs (~20
541 kDa) and VAMPs (~14 kDa). This was to ensure that the presence of other high
542 abundance and high molecular weight proteins did not mask these low abundant low
543 molecular weight proteins. We identified 17 different RABs on the phagosomes out of
544 which nine were associated with Golgi function. We also identified five out of six
545 known ARFs, where ARF1 and ARF3 were particularly important for their known
546 association with Golgi apparatus, phagosome/engulfment and exocytosis(Beck et al.,
547 2008; Faundez et al., 1997; Krauss et al., 2008). We could identify four different

548 VAMPs in the phagosomes including VAMP2, 3, 4 and 8. While role of VAMP3 in
549 phagosome biogenesis is well described, VAMP2 is particularly known for its
550 involvement in exocytosis, neurotransmitter release and secretory vesicles (Faurschou
551 and Borregaard, 2003; Shen et al., 2015). Previously in a proteomic study of the latex-
552 beads containing phagosome, VAMP4 was identified as phagosome membrane
553 associated protein (Shui et al., 2008). VAMP4 are trans-Golgi resident proteins and
554 are also involved in the immature secretory granules (Steegmaier et al., 1999). We
555 also found SEC22B in the phagosome MS data, an important SNARE known to be
556 important for the recruitment of ER during phagocytic uptake (Becker et al., 2005).
557 Considering the number of RABs, ARFs and VAMPs associated with the exocytosis
558 and secretory vesicles, it seems very likely that the true identity of the Golgi-derived
559 vesicles that are recruited during phagosome biogenesis could be secretory vesicles.
560 However the role of GA during phagocytosis was ruled out in the past since
561 phagocytic uptake was found insensitive to Brefeldin A (Becker et al., 2005), a fungal
562 metabolite, which disrupts the GA (Lippincott-Schwartz et al., 1989). Interestingly
563 during membrane repair process, which is also dependent on secretory vesicles from
564 GA in addition to other membrane sources, while the repair of first wound is typically
565 independent of Brefeldin A, it has been reported that repair of any subsequent wounds
566 are sensitive to Brefeldin A (Andrews, 2002; Togo et al., 2000). Similarly during
567 secretion, Brefeldin A while inhibits the formation of new secretory vesicles, does not
568 interfere with the membrane fusion of pre-formed vesicles (Miller et al., 1992; Rosa
569 et al., 1992). Thus it is possible that following exhaustion of pre-formed vesicles
570 during phagocytosis, uptake of any subsequent cargo encountered by the cell may
571 show sensitivity to BFA. This is an interesting proposition and certainly warrants
572 further investigations.

573 At the molecular level it seems SNARE mediated fusion may be involved in the
574 phagosome biogenesis. We were able to track the presence of syntaxin 1, the t-
575 SNARE at the plasma membrane involved in SNARE mediated vesicle fusion, along
576 with Mannosidase-II at the early phagosomes (Fig S7D). Syntaxin-1 is known to
577 facilitate fusion of secretory vesicles(Sollner et al., 1993). Moreover, its presence will
578 also be required for the fusion of VAMP3 positive vesicles, a vSNARE typically
579 located in the recycling endosomes. Given the multiplicity of v-SNAREs and t-
580 SNAREs with possibly overlapping functions makes it challenging to clearly establish
581 the fusion machinery involved. The identity of SNAREs involved in this process
582 therefore constitutes the next set of challenge following this study. Taken together the
583 results in this study allowed us to reconstruct the process of phagocytosis (Fig. 7E).
584 We note that Golgi-derived vesicles are one of the several sub-cellular vesicular pools
585 available for phagosome biogenesis including recycling endosomes and lysosomes. It
586 actually explains why in many cases except for PI3K inhibition, the effects were more
587 kinetic in nature. We did observe in our results cases where some phagosomes were
588 only positive for VAMP3 and not Mannosidase-II or vice-versa, leaving us with an
589 intriguing question that whether the outcome of phagocytosis could vary depending
590 on which organelle contributed the most for the formation of phagosome.
591 In conclusion, we show here an as yet unknown function of Golgi-derived vesicles
592 during phagocytic uptake in macrophages. The targeted exocytosis coupled with
593 phagocytosis has been studied in the past, however involvement of vesicles from the
594 GA in macrophages is unprecedented. Similarly regulation of phagocytic uptake by
595 NCS1 comprehensively extends the known functions of this molecule in
596 macrophages. Finally our finding that the voltage-gated Ca^{2+} channel could play a
597 role in the process of phagocytosis may be potentially harnessed in future for

598 developing better therapeutic interventions for various infectious diseases including
599 tuberculosis.
600

601 # Methods

602 ## Ethics statement

603 The animal experiments were performed upon prior approval from the institutional
604 ethics committee (IAEC) of International Center for Genetic Engineering and
605 Biotechnology (Approval no.: ICGEB/AH/2013/03/IMM-38).

606 **Reagents And Antibodies:** The following reagents were used in this study:
607 Wortmannin (Sigma Aldrich,W1628), Dynasore Hydrate (Sigma Aldrich, D7693),
608 Nocodazole (Sigma Aldrich, M1404), TMB8 (Sigma Aldrich, T111), EGTA
609 (Amresco, 0732), Loperamide (Sigma Aldrich, L4762), Amlodipine besylate (Sigma
610 Aldrich, A5605), PKH 67 (Sigma Aldrich, MINI 26), RIPA buffer (Amresco,N653),
611 BSA (Sigma Aldrich, A2153), Saponin (Sigma Aldrich, 47036), Puromycin
612 (Invivogen, ant-pr-1), 4 µm aldehydate-sulphatelatex beads (Life Technologies,
613 A37304) and 1µm yellow green aldehyde latex beads (Life Technologies, F8823).
614 All the siRNA used in this study were siGenome siRNA SmartPool (Dharmacon Inc).
615 The transfection reagent used for siRNA transfections was Dharmafect-2 (Dharmacon
616 Inc). The primary antibodies used in this study are: Mannosidase II (abcam, ab12277),
617 Dynamin (Santacruz, sc-6401), VAMP3 (abcam, ab43080), Transferrin (abcam,
618 ab84036). The secondary antibodies used in this study are: Alexa fluor 405 and Alexa
619 fluor 568 conjugates from (Life Technologies). **Plasmid Constructs:** The plasmid
620 constructs used in this study are mCherry-ManII-N-10 (Addgene plasmid #55073),
621 pcDNA3.1_AktPH-mCherry (Addgene plasmid #67301), pCT- Golgi-GFP
622 (CYTO104-VA-1) and pCT-Mem-GFP (System Biosciences, CYTO100-PA-1).

623 **Bacterial Culture Maintainence:** Mycobacterial cultures were maintained in 7H9
624 media (Difco) supplemented with 10% OADC. Single cell suspension of
625 Mycobacterial strains were prepared by aspiration of the culture eight times with 26
626 gauge needle and six times 30 gauge needles. Quantification of this prepared culture
627 was done by taking absorbance at 600 nm wavelength (0.6 O.D. corresponds to ~100
628 x 10^6 bacteria). The bacteria thus appropriately calculated were added to the cells at
629 the mentioned MOI (Multiplicity of Infection). For microscopy experiments, the
630 desired number of bacteria was stained with PKH67 (Sigma Aldrich), a lipophilic
631 green fluorescent dye, as per the manufacturer's protocol. The stained bacteria were
632 then passed thrice through a 26-gauge needle and used for infection. *E. coli* and
633 *Salmonella* Typhimurium strains were maintained in LB (Difco). For infection culture
634 density was determined by OD at 600 for both *E. coli* and *S.*Typhimurium containing
635 GFP, an OD of 1= 1 x 10^8 bacteria for both these strains.
636 **Tissue Culture:** THP-1 cells (a kind gift from Dr. Dong An, UCLA) and U937 cells
637 (ATCC) were cultured in RPMI 1640 medium (Life Technologies) and RAW264.7
638 (ATCC) murine macrophages were grown in Dulbecco's modified Eagle's media
639 (DMEM, Life Technologies) supplemented with 10% Fetal Bovine Serum (FBS,
640 GIBCO) and maintained 37°C in a humidified, 5% CO_2 atmosphere. THP1 cells were
641 differentiated with 20ng/µl PMA for 24 hours, washed with plain RPMI and
642 maintained in 10% FCS supplemented RPMI for another 24 hours. The cells were
643 then infected with respective bacteria/beads. RAW264.7 macrophages were seeded in
644 respective plates and differentiated with 200ng/ml LPS for 12 hours. The cells were
645 washed once with plain DMEM and infected with respective bacteria/beads.
646 **Animals and isolation of BMDMs**

647 Bone marrow derived macrophages (BMDMs) were isolated from femurs of BALB/C
648 mice (4-6 weeks old, female) obtained from institutional animal house. BMDMs were
649 obtained by culturing the marrow cells in the presence of macrophage-colony
650 stimulating factor (M-CSF, eBioscience, 14-8983-80) for 7 days. Fully differentiated
651 macrophages were harvested and seeded for infection with H37Rv. The infection
652 protocol was same as described above for THP-1 macrophages.
653
654 **Experiments with Latex beads:** For microscopy experiments 4µm aldehyde sulfate
655 latex beads (Life Technologies) were incubated with human/mouse IgG on an agitator
656 overnight. The beads were washed twice with plain DMEM by centrifugation at 2000
657 rpm for 10 minutes and added to cells at respective MOI. For flow cytometry
658 experiments, 1µm FITC labeled aldehyde beads were added at respective MOI to the
659 differentiated THP1 cells.
660 **Transfection & Nucleofection Assays:** Transfection & Transduction was carried out
661 using JetPrime Reagent (Himedia) as per the manufacturer's protocol. Nucleofection
662 was carried out with the 4D-Nucleofector™ System Lonza in 20 µl Nucleocuvette™
663 Strips with program DS-136, as per the manufacturer's protocol. At 24 hours post
664 Nucleofection these cells expressed the inserted vector as determined by visualization
665 with a fluorescence microscope.
666 **siRNA Transfection & Inhibitor Assays:** Post 24 hours of PMA treatment, the cells
667 were washed once with plain RPMI. The siRNA's were added as per the
668 manufacturer's protocol. Post 48 hours of incubation the respective infection/assays
669 were performed. For the inhibitor assays such as, Dynasore(40µM, 80µM),
670 Wortmannin (as specified) were added 4 hours before infection. While
671 Nocodazole(25 µM) was added 2.5 hours before infection and EGTA(3mM),

672 TMB8(100 μM), Loperamide hydrochloride(100 μM) and Amlodipine besylate(100
673 μM) were added for 30 minutes before infection.

674 **Creation of stable cell lines:** The stable cell lines were created from lentivirus
675 cytotracer plasmids (B4GALT1-mRuby and NEUM-EGFP, System Biosciences).
676 $1X10^6$ U937 cells were added to a 24 well plate. The harvested media containing
677 lentivirus (refer to transfection section) was added to them. At 72 hours post infection
678 the cells were selected on Puromycin at 350ng/ml for 21 days. The population of
679 positive cells was routinely checked by microscopy and it was found that post
680 selection for 21 days the population of cells remained stable (in our case 30-40%).

681 **Staining for Confocal Microscopy:** At specific time points cells were fixed with 4%
682 Paraformaldehyde (PFA) for 15 minutes. This was followed by 2 washes with 1x
683 PBS. The cells were permeabilized with 0.4% Triton X- 100 for 30 minutes and
684 washed once with 1X PBS. Blocking was performed using 3 %(w/v) BSA and
685 0.5%Tween-20 in 1X PBS for one hour, followed by one wash with 1X PBS. The
686 cells were now stained with respective primary antibody made in the blocking
687 solution at specific dilution for 90 minutes. The coverslips were then washed once
688 with 1X PBST and twice with 1X PBS. This was followed by staining with respective
689 secondary antibody tagged with fluorophore of choice for 90 minutes. The primary
690 and secondary antibodies were diluted in blocking solutions for use. After three
691 washes with 1X PBS, the coverslips were then mounted on glass slides with anti-fade
692 reagent(Life Technologies). Images were acquired with Nikon A1R Laser Scanning
693 Confocal Microscope with a 100X/1.4NA Plan Apochromat VC, DIC N2 objective
694 lens. Image processing viz. 3D reconstruction, co-localization and intensity
695 measurements were done via Imaris 7.2 (Bitplane).

696 **Live Cell Imaging:** The live cell imaging dish pre-seeded was RAW264.7
697 macrophages expressing mCherry-MAN2A. The live cell system was set at 5% CO_2
698 and 37^0C. The field was set and imaged for 10 minutes. This was followed by an on-
699 stage addition of 0.0001% saponin for 5 minutes. The cells were washed once,
700 supplemented with complete media and imagining continued. The entire procedure
701 was performed on stage to analyze the pre- and post treatment effects on the
702 membrane under our experimental set up.

703 **Flow Cytometry experiments:** At respective time points, the infected cells were
704 washed thrice with sterile 1X PBS to remove extracellular bacteria/beads and fixed
705 with 2% PFA. The cells were scraped and run on BD FACS Canto or BD FACS
706 Influx cytometer's.

707 **Western Blot:** Post SDS PAGE, the proteins were blotted onto a nitrocellulose
708 membrane using a semidry-transfer system. Following incubation with primary and
709 secondary antibodies, the blots were scanned using Odyssey InfraRed Imaging
710 System (LI-COR BioSciences, Lincoln, NE, USA) at various intensities in order to
711 obtain a blot scan with minimum background. All settings were rigorously maintained
712 for all experiments. The scans were quantitatively analyzed using Odyssey InfraRed
713 Imaging System Application Software_Version.3.O (commercially available from (LI-
714 COR BioSciences, Lincoln, NE, USA).

715 **Phagosome Isolation:** Latex bead phagosome for 1μm latex beads were isolated as
716 per protocol described earlier (Desjardins et al., 1994). At 1 hour post addition, the
717 plates were washed 4 times with cold 1XPBS, ensuring all the extracellular beads
718 were completely washed off. The cells were scraped off with a rubber policeman and
719 centrifuged twice with cold 1XPBS at 1200 RPM for 5 minutes. The cells were
720 pooled and washed once with homogenization buffer at 1200 RPM for 5 Minutes

721 (3mM imidazole, 250 mM sucrose, pH 7.4). The cells were then incubated in
722 appropriate volume of homogenization buffer (with protease inhibitor cocktail –
723 Amresco) for 30 minutes. The cells were lysed by dounce homogenizer till 90% of the
724 cells were disrupted as observed under a light microscope. This lysate was
725 centrifuged at 1200 RPM for 5 minutes at 4^0C to remove the unbroken cells. This was
726 followed by preparation of sucrose gradient for ultracentrifugation. The homogenate
727 was made to be consisting of 40% sucrose by mixing with equal volume of 62%
728 sucrose and 2.25 ml of the same was layered upon 2.0ml of 62% sucrose solution. We
729 then added 2.25 ml each of 35%, 25% and 10% sucrose solutions. The tubes were
730 centrifuged at 100,000g for 1 hour at 4^0C in an SW28 rotor (Beckman Coulter). The
731 LBC band obtained between 10 and 25% sucrose layers was collected and washed
732 once with cold 1XPBS at 40,000g at 4^0C in an SW28 rotor (Beckman Coulter).
733 **Mass Spectrometry & Data Analysis:** For LC-LTQ Orbitrap MS analysis, samples
734 were re-solubilized in 2% [v/v] acetonitrile, 0.1% [v/v] formic acid in water and
735 injected onto the trap column at a flow rate of 20 µl/min subsequently peptides were
736 separated on Zorbax 300SB-C18 (Agilent, Santa Clara, CA, USA) by a gradient
737 developed from 2% [v/v] acetonitrile, 0.1% [v/v] formic acid to 80% [v/v]
738 acetonitrile, 0.1% [v/v] formic acid in water over 180 min at a flow rate of 300 nl/min
739 onto an Agilent 1200 (Agilent, Santa Clara, CA, USA) nano-flow LC-System that
740 was in-line coupled to the nano-electrospray source of a LTQ-Orbitrap discovery
741 hybrid mass spectrometer (Thermo Scientific, San Jose, CA, USA). Full MS in a mass
742 range between m/z 300-2,000 was performed in the Orbitrap mass analyzer with a
743 resolution of 30,000 at m/z 400 and an AGC target of 2x 105. The strongest five
744 signals were selected for CID (collision induced dissociation)-MS/MS in the LTQ ion
745 trap at a normalized collision energy of 35% using an AGC target of 1x 105 and two

746 microscans. Dynamic exclusion was enabled with one repeat counts during 45 s and
747 an exclusion period of 180 s. Peptide identification was performed by CID-based
748 MS/MS of the selected precursors. For protein/peptide identification, MS/MS data
749 were searched against the *Mus musculus* amino acid sequence database (downloaded
750 in August 2015) using an in-house Mascot server (version 2.4) through the Proteome
751 Discoverer 1.4 software. The search was set up for full tryptic peptides with a
752 maximum of three missed cleavage sites- carbamidomethyl on cysteine, and oxidized
753 methionine were included as variable modifications. The precursor mass tolerance
754 threshold was 10 ppm, and the maximum fragment mass error was 0.8 Da. The
755 significance threshold of the ion score was calculated based on a false discovery rate
756 of <1%, estimated by the peptide validator node of the Proteome Discoverer software.

757 **Analysis for functional classes:**

758 The non-redundant list of proteins identified was matched against a series of gene
759 ontology classes from AMIGO2 database. The selection of gene ontology was
760 empirically made based on known and perceived classes, which together could
761 represent the set of trafficking proteins identified. The obtained matches were then
762 represented as a network using Cytoscape 3.2.0.

763 **Statistical Analysis:**

764 Comparative groups were analyzed using paired two-tailed t-test using inbuilt
765 function in MS Excel.

766 **3-D recreation and analysis:** The intensity of a particular fluorophore on the bead
767 was estimated by first creating a three dimensional bead surface in the captured image
768 (z-stack) using "spot module" in Imaris Version 7.2 (Bitplane) which automatically
769 detects spheres in an image depending upon the dimensions fed. The software then
770 allows one to determine fluorescence intensity on the surface individually for each

771 fluorophore. For each case maximum fluorescence intensity was determined and
772 plotted.

773 **PIP3 gradient analysis:** The gradient of fluorescence in the AKT-pH mCherry
774 experiments was determined using "intensity profile line tool" in NIS-Elements
775 (NIKON).

776 **ACKNOWLEDGEMENTS**

777 The work was supported by a grant from the Department of Biotechnology (DBT),
778 Govt. of India (BT/PR14730/BRB/10/874/2010, DK) and partly by International
779 AIDS Society and CFAR funded CNIHR grant from NIH, USA (DK). The work
780 related to *Mycobacterium tuberculosis* infections were carried out at DBT funded
781 TACF facility at ICGEB. We thank Prof. Sarman Singh for access to the flow-
782 cytometer at AIIMS and Purnima for her help in the confocal microscopy. We thank
783 C-CAMP, NCBS, Bangalore for the mass spectrometry facility. NV is a recipient of a
784 senior research fellowship from the University Grants Commission, India.

785 **References**

786

787 Achiriloaie, M., B. Barylko, and J.P. Albanesi. 1999. Essential role of the dynamin
788 pleckstrin homology domain in receptor-mediated endocytosis. *Molecular*
789 *and cellular biology*. 19:1410-1415.
790 Aderem, A., and D.M. Underhill. 1999. Mechanisms of phagocytosis in
791 macrophages. *Annual review of immunology*. 17:593-623.
792 Alix, E., S. Mukherjee, and C.R. Roy. 2011. Subversion of membrane transport
793 pathways by vacuolar pathogens. *The Journal of cell biology*. 195:943-952.
794 Andrews, N.W. 2002. Lysosomes and the plasma membrane: trypanosomes
795 reveal a secret relationship. *The Journal of cell biology*. 158:389-394.
796 Augustine, G.J. 2001. How does calcium trigger neurotransmitter release?
797 *Current opinion in neurobiology*. 11:320-326.
798 Bainton, D.F., R. Takemura, P.E. Stenberg, and Z. Werb. 1989. Rapid
799 fragmentation and reorganization of Golgi membranes during frustrated
800 phagocytosis of immobile immune complexes by macrophages. *The*
801 *American journal of pathology*. 134:15-26.
802 Bajno, L., X.R. Peng, A.D. Schreiber, H.P. Moore, W.S. Trimble, and S. Grinstein.
803 2000. Focal exocytosis of VAMP3-containing vesicles at sites of
804 phagosome formation. *The Journal of cell biology*. 149:697-706.
805 Beck, R., Z. Sun, F. Adolf, C. Rutz, J. Bassler, K. Wild, I. Sinning, E. Hurt, B. Brugger,
806 J. Bethune, and F. Wieland. 2008. Membrane curvature induced by Arf1-

807 GTP is essential for vesicle formation. *Proceedings of the National*
808 *Academy of Sciences of the United States of America*. 105:11731-11736.
809 Becker, T., A. Volchuk, and J.E. Rothman. 2005. Differential use of endoplasmic
810 reticulum membrane for phagocytosis in J774 macrophages. *Proceedings*
811 *of the National Academy of Sciences of the United States of America*.
812 102:4022-4026.
813 Beemiller, P., A.D. Hoppe, and J.A. Swanson. 2006. A phosphatidylinositol-3-
814 kinase-dependent signal transition regulates ARF1 and ARF6 during
815 Fcgamma receptor-mediated phagocytosis. *PLoS biology*. 4:e162.
816 Behar, S.M., M. Divangahi, and H.G. Remold. 2010. Evasion of innate immunity by
817 Mycobacterium tuberculosis: is death an exit strategy? *Nature reviews.*
818 *Microbiology*. 8:668-674.
819 Bonifacino, J.S., and B.S. Glick. 2004. The mechanisms of vesicle budding and
820 fusion. *Cell*. 116:153-166.
821 Braun, V., C. Deschamps, G. Raposo, P. Benaroch, A. Benmerah, P. Chavrier, and F.
822 Niedergang. 2007. AP-1 and ARF1 control endosomal dynamics at sites of
823 FcR mediated phagocytosis. *Molecular biology of the cell*. 18:4921-4931.
824 Braun, V., and F. Niedergang. 2006. Linking exocytosis and endocytosis during
825 phagocytosis. *Biology of the cell / under the auspices of the European Cell*
826 *Biology Organization*. 98:195-201.
827 Cannon, G.J., and J.A. Swanson. 1992. The macrophage capacity for phagocytosis.
828 *Journal of cell science*. 101 (Pt 4):907-913.
829 Carrithers, M.D., G. Chatterjee, L.M. Carrithers, R. Offoha, U. Iheagwara, C. Rahner,
830 M. Graham, and S.G. Waxman. 2009. Regulation of podosome formation in
831 macrophages by a splice variant of the sodium channel SCN8A. *The*
832 *Journal of biological chemistry*. 284:8114-8126.
833 Chen, Y.A., and R.H. Scheller. 2001. SNARE-mediated membrane fusion. *Nature*
834 *reviews. Molecular cell biology*. 2:98-106.
835 Church, J., E.J. Fletcher, K. Abdel-Hamid, and J.F. MacDonald. 1994. Loperamide
836 blocks high-voltage-activated calcium channels and N-methyl-D-
837 aspartate-evoked responses in rat and mouse cultured hippocampal
838 pyramidal neurons. *Molecular pharmacology*. 45:747-757.
839 Cox, D., C.C. Tseng, G. Bjekic, and S. Greenberg. 1999. A requirement for
840 phosphatidylinositol 3-kinase in pseudopod extension. *The Journal of*
841 *biological chemistry*. 274:1240-1247.
842 Czibener, C., N.M. Sherer, S.M. Becker, M. Pypaert, E. Hui, E.R. Chapman, W.
843 Mothes, and N.W. Andrews. 2006. Ca2+ and synaptotagmin VII-dependent
844 delivery of lysosomal membrane to nascent phagosomes. *The Journal of*
845 *cell biology*. 174:997-1007.
846 Dai, S., Y. Zhang, T. Weimbs, M.B. Yaffe, and D. Zhou. 2007. Bacteria-generated
847 PtdIns(3)P recruits VAMP8 to facilitate phagocytosis. *Traffic*. 8:1365-
848 1374.
849 Desjardins, M., L.A. Huber, R.G. Parton, and G. Griffiths. 1994. Biogenesis of
850 phagolysosomes proceeds through a sequential series of interactions with
851 the endocytic apparatus. *The Journal of cell biology*. 124:677-688.
852 Di, A., D.J. Nelson, V. Bindokas, M.E. Brown, F. Libunao, and H.C. Palfrey. 2003.
853 Dynamin regulates focal exocytosis in phagocytosing macrophages.
854 *Molecular biology of the cell*. 14:2016-2028.

855 Divangahi, M., M. Chen, H. Gan, D. Desjardins, T.T. Hickman, D.M. Lee, S. Fortune,
856 S.M. Behar, and H.G. Remold. 2009. Mycobacterium tuberculosis evades
857 macrophage defenses by inhibiting plasma membrane repair. *Nature*
858 *immunology*. 10:899-906.
859 Drecktrah, D., L.A. Knodler, R. Ireland, and O. Steele-Mortimer. 2006. The
860 mechanism of Salmonella entry determines the vacuolar environment and
861 intracellular gene expression. *Traffic*. 7:39-51.
862 Faundez, V., J.T. Horng, and R.B. Kelly. 1997. ADP ribosylation factor 1 is required
863 for synaptic vesicle budding in PC12 cells. *The Journal of cell biology*.
864 138:505-515.
865 Faurschou, M., and N. Borregaard. 2003. Neutrophil granules and secretory
866 vesicles in inflammation. *Microbes and infection / Institut Pasteur*. 5:1317-
867 1327.
868 Flannagan, R.S., V. Jaumouille, and S. Grinstein. 2012. The cell biology of
869 phagocytosis. *Annual review of pathology*. 7:61-98.
870 Funamoto, S., R. Meili, S. Lee, L. Parry, and R.A. Firtel. 2002. Spatial and temporal
871 regulation of 3-phosphoinositides by PI 3-kinase and PTEN mediates
872 chemotaxis. *Cell*. 109:611-623.
873 Gagnon, E., S. Duclos, C. Rondeau, E. Chevet, P.H. Cameron, O. Steele-Mortimer, J.
874 Paiement, J.J. Bergeron, and M. Desjardins. 2002. Endoplasmic reticulum-
875 mediated phagocytosis is a mechanism of entry into macrophages. *Cell*.
876 110:119-131.
877 Gillingham, A.K., and S. Munro. 2007. The small G proteins of the Arf family and
878 their regulators. *Annual review of cell and developmental biology*. 23:579-
879 611.
880 Gillingham, A.K., and S. Munro. 2016. Finding the Golgi: Golgin Coiled-Coil
881 Proteins Show the Way. *Trends in cell biology*.
882 Gold, E.S., D.M. Underhill, N.S. Morrissette, J. Guo, M.A. McNiven, and A. Aderem.
883 1999. Dynamin 2 is required for phagocytosis in macrophages. *The*
884 *Journal of experimental medicine*. 190:1849-1856.
885 Haynes, L.P., G.M. Thomas, and R.D. Burgoyne. 2005. Interaction of neuronal
886 calcium sensor-1 and ADP-ribosylation factor 1 allows bidirectional
887 control of phosphatidylinositol 4-kinase beta and trans-Golgi network-
888 plasma membrane traffic. *The Journal of biological chemistry*. 280:6047-
889 6054.
890 Henley, J.R., and M.A. McNiven. 1996. Association of a dynamin-like protein with
891 the Golgi apparatus in mammalian cells. *The Journal of cell biology*.
892 133:761-775.
893 Holevinsky, K.O., and D.J. Nelson. 1998. Membrane capacitance changes
894 associated with particle uptake during phagocytosis in macrophages.
895 *Biophysical journal*. 75:2577-2586.
896 Jones, S.M., K.E. Howell, J.R. Henley, H. Cao, and M.A. McNiven. 1998. Role of
897 dynamin in the formation of transport vesicles from the trans-Golgi
898 network. *Science*. 279:573-577.
899 Jutras, I., and M. Desjardins. 2005. Phagocytosis: at the crossroads of innate and
900 adaptive immunity. *Annual review of cell and developmental biology*.
901 21:511-527.
902 Kochegarov, A.A. 2003. Pharmacological modulators of voltage-gated calcium
903 channels and their therapeutical application. *Cell calcium*. 33:145-162.

904 Koul, A., T. Herget, B. Klebl, and A. Ullrich. 2004. Interplay between mycobacteria
905 and host signalling pathways. *Nature reviews. Microbiology*. 2:189-202.
906 Krauss, M., J.Y. Jia, A. Roux, R. Beck, F.T. Wieland, P. De Camilli, and V. Haucke.
907 2008. Arf1-GTP-induced tubule formation suggests a function of Arf
908 family proteins in curvature acquisition at sites of vesicle budding. *The*
909 *Journal of biological chemistry*. 283:27717-27723.
910 Kreitzer, G., A. Marmorstein, P. Okamoto, R. Vallee, and E. Rodriguez-Boulan.
911 2000. Kinesin and dynamin are required for post-Golgi transport of a
912 plasma-membrane protein. *Nature cell biology*. 2:125-127.
913 Lee, W.L., R.E. Harrison, and S. Grinstein. 2003. Phagocytosis by neutrophils.
914 *Microbes and infection / Institut Pasteur*. 5:1299-1306.
915 Link, T.M., U. Park, B.M. Vonakis, D.M. Raben, M.J. Soloski, and M.J. Caterina. 2010.
916 TRPV2 has a pivotal role in macrophage particle binding and
917 phagocytosis. *Nature immunology*. 11:232-239.
918 Lippincott-Schwartz, J., L.C. Yuan, J.S. Bonifacino, and R.D. Klausner. 1989. Rapid
919 redistribution of Golgi proteins into the ER in cells treated with brefeldin
920 A: evidence for membrane cycling from Golgi to ER. *Cell*. 56:801-813.
921 Liu, Y.C., E.R. Chapman, and D.R. Storm. 1991. Targeting of neuromodulin (GAP-
922 43) fusion proteins to growth cones in cultured rat embryonic neurons.
923 *Neuron*. 6:411-420.
924 Lundqvist-Gustafsson, H., M. Gustafsson, and C. Dahlgren. 2000. Dynamic
925 ca(2+)changes in neutrophil phagosomes A source for intracellular
926 ca(2+)during phagolysosome formation? *Cell calcium*. 27:353-362.
927 Miller, S.G., L. Carnell, and H.H. Moore. 1992. Post-Golgi membrane traffic:
928 brefeldin A inhibits export from distal Golgi compartments to the cell
929 surface but not recycling. *The Journal of cell biology*. 118:267-283.
930 Miyake, K., and P.L. McNeil. 1995. Vesicle accumulation and exocytosis at sites of
931 plasma membrane disruption. *The Journal of cell biology*. 131:1737-1745.
932 Niedergang, F., and P. Chavrier. 2004. Signaling and membrane dynamics during
933 phagocytosis: many roads lead to the phagos(R)ome. *Current opinion in*
934 *cell biology*. 16:422-428.
935 Praefcke, G.J., and H.T. McMahon. 2004. The dynamin superfamily: universal
936 membrane tubulation and fission molecules? *Nature reviews. Molecular*
937 *cell biology*. 5:133-147.
938 Reddy, A., E.V. Caler, and N.W. Andrews. 2001. Plasma membrane repair is
939 mediated by Ca(2+)-regulated exocytosis of lysosomes. *Cell*. 106:157-169.
940 Ridley, A.J., M.A. Schwartz, K. Burridge, R.A. Firtel, M.H. Ginsberg, G. Borisy, J.T.
941 Parsons, and A.R. Horwitz. 2003. Cell migration: integrating signals from
942 front to back. *Science*. 302:1704-1709.
943 Rosa, P., F.A. Barr, J.C. Stinchcombe, C. Binacchi, and W.B. Huttner. 1992.
944 Brefeldin A inhibits the formation of constitutive secretory vesicles and
945 immature secretory granules from the trans-Golgi network. *European*
946 *journal of cell biology*. 59:265-274.
947 Samie, M., X. Wang, X. Zhang, A. Goschka, X. Li, X. Cheng, E. Gregg, M. Azar, Y.
948 Zhuo, A.G. Garrity, Q. Gao, S. Slaugenhaupt, J. Pickel, S.N. Zolov, L.S.
949 Weisman, G.M. Lenk, S. Titus, M. Bryant-Genevier, N. Southall, M. Juan, M.
950 Ferrer, and H. Xu. 2013. A TRP channel in the lysosome regulates large
951 particle phagocytosis via focal exocytosis. *Developmental cell*. 26:511-524.

952 Scalettar, B.A., P. Rosa, E. Taverna, M. Francolini, T. Tsuboi, S. Terakawa, S.
953 Koizumi, J. Roder, and A. Jeromin. 2002. Neuronal calcium sensor-1 binds
954 to regulated secretory organelles and functions in basal and stimulated
955 exocytosis in PC12 cells. *Journal of cell science*. 115:2399-2412.
956 Shen, C., S.S. Rathore, H. Yu, D.R. Gulbranson, R. Hua, C. Zhang, N.E. Schoppa, and
957 J. Shen. 2015. The trans-SNARE-regulating function of Munc18-1 is
958 essential to synaptic exocytosis. *Nature communications*. 6:8852.
959 Shui, W., L. Sheu, J. Liu, B. Smart, C.J. Petzold, T.Y. Hsieh, A. Pitcher, J.D. Keasling,
960 and C.R. Bertozzi. 2008. Membrane proteomics of phagosomes suggests a
961 connection to autophagy. *Proceedings of the National Academy of Sciences*
962 *of the United States of America*. 105:16952-16957.
963 Singh, D.K., D. Kumar, Z. Siddiqui, S.K. Basu, V. Kumar, and K.V. Rao. 2005. The
964 strength of receptor signaling is centrally controlled through a
965 cooperative loop between Ca2+ and an oxidant signal. *Cell*. 121:281-293.
966 Sollner, T., S.W. Whiteheart, M. Brunner, H. Erdjument-Bromage, S. Geromanos, P.
967 Tempst, and J.E. Rothman. 1993. SNAP receptors implicated in vesicle
968 targeting and fusion. *Nature*. 362:318-324.
969 Steegmaier, M., J. Klumperman, D.L. Foletti, J.S. Yoo, and R.H. Scheller. 1999.
970 Vesicle-associated membrane protein 4 is implicated in trans-Golgi
971 network vesicle trafficking. *Molecular biology of the cell*. 10:1957-1972.
972 Steinhardt, R.A., G. Bi, and J.M. Alderton. 1994. Cell membrane resealing by a
973 vesicular mechanism similar to neurotransmitter release. *Science*.
974 263:390-393.
975 Stendahl, O., K.H. Krause, J. Krischer, P. Jerstrom, J.M. Theler, R.A. Clark, J.L.
976 Carpentier, and D.P. Lew. 1994. Redistribution of intracellular Ca2+ stores
977 during phagocytosis in human neutrophils. *Science*. 265:1439-1441.
978 Stenmark, H. 2009. Rab GTPases as coordinators of vesicle traffic. *Nature reviews.*
979 *Molecular cell biology*. 10:513-525.
980 Sudhof, T.C. 2012. Calcium control of neurotransmitter release. *Cold Spring*
981 *Harbor perspectives in biology*. 4:a011353.
982 Tardieux, I., P. Webster, J. Ravesloot, W. Boron, J.A. Lunn, J.E. Heuser, and N.W.
983 Andrews. 1992. Lysosome recruitment and fusion are early events
984 required for trypanosome invasion of mammalian cells. *Cell*. 71:1117-
985 1130.
986 Togo, T., J.M. Alderton, G.Q. Bi, and R.A. Steinhardt. 1999. The mechanism of
987 facilitated cell membrane resealing. *Journal of cell science*. 112 (Pt 5):719-
988 731.
989 Togo, T., T.B. Krasieva, and R.A. Steinhardt. 2000. A decrease in membrane
990 tension precedes successful cell-membrane repair. *Molecular biology of*
991 *the cell*. 11:4339-4346.
992 Underhill, D.M., and A. Ozinsky. 2002. Phagocytosis of microbes: complexity in
993 action. *Annual review of immunology*. 20:825-852.
994 Velasco, A., L. Hendricks, K.W. Moremen, D.R. Tulsiani, O. Touster, and M.G.
995 Farquhar. 1993. Cell type-dependent variations in the subcellular
996 distribution of alpha-mannosidase I and II. *The Journal of cell biology*.
997 122:39-51.
998 Vicker, M.G. 1977. On the origin of the phagocytic membrane. *Experimental cell*
999 *research*. 109:127-138.

1000 Vinet, A.F., M. Fukuda, and A. Descoteaux. 2008. The exocytosis regulator
1001 synaptotagmin V controls phagocytosis in macrophages. *Journal of*
1002 *immunology*. 181:5289-5295.
1003 Warnock, D.E., T. Baba, and S.L. Schmid. 1997. Ubiquitously expressed dynamin-
1004 II has a higher intrinsic GTPase activity and a greater propensity for self-
1005 assembly than neuronal dynamin-I. *Molecular biology of the cell*. 8:2553-
1006 2562.
1007 Zhang, Q., D. Cox, C.C. Tseng, J.G. Donaldson, and S. Greenberg. 1998. A
1008 requirement for ARF6 in Fcgamma receptor-mediated phagocytosis in
1009 macrophages. *The Journal of biological chemistry*. 273:19977-19981.
1010 Zuchner, S., M. Noureddine, M. Kennerson, K. Verhoeven, K. Claeys, P. De Jonghe,
1011 J. Merory, S.A. Oliveira, M.C. Speer, J.E. Stenger, G. Walizada, D. Zhu, M.A.
1012 Pericak-Vance, G. Nicholson, V. Timmerman, and J.M. Vance. 2005.
1013 Mutations in the pleckstrin homology domain of dynamin 2 cause
1014 dominant intermediate Charcot-Marie-Tooth disease. *Nature genetics*.
1015 37:289-294.
1016

Figure 1

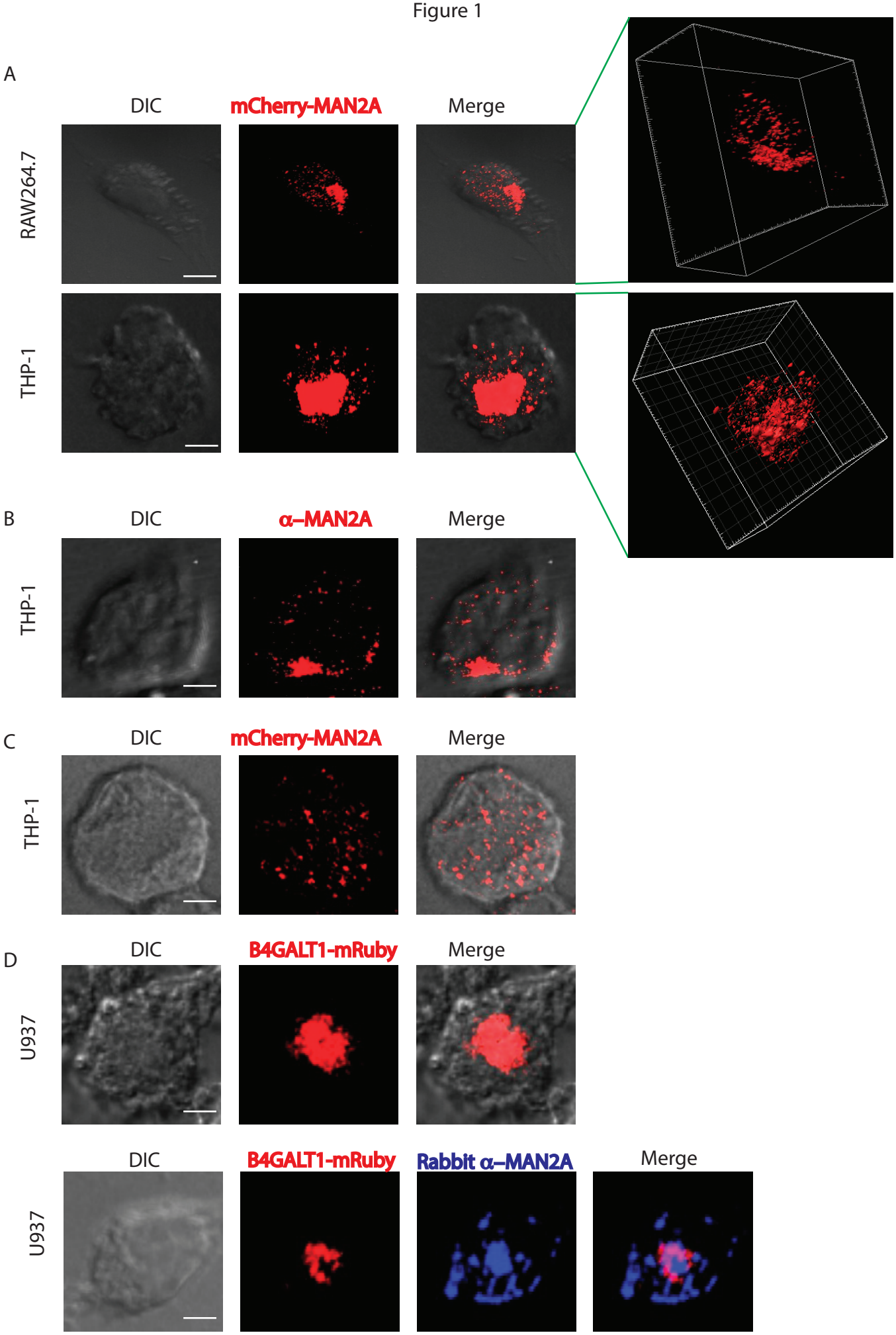
A
DIC
mCherry-MAN2A
Merge
RAW264.7
THP-1
B
DIC
α–MAN2A
Merge
THP-1
C
DIC
mCherry-MAN2A
Merge
THP-1
D
DIC
B4GALT1-mRuby
Merge
U937
DIC
B4GALT1-mRuby
Rabbit α–MAN2A
Merge
U937

1017 **FIGURE LEGENDS**

1018 **Figure 1: Mannosidase-II is a marker of Golgi apparatus and vesicles derived**
1019 **from the Golgi**

1020 A) RAW264.7 cells and THP-1 derived macrophages were nucleofected with
1021 mCherry-MAN2A. At 24 hours post nucleofection, cells were visualized under the
1022 confocal microscope (see methods for detail). The 3-D plots at the right were created
1023 using Imaris 7.2 software tool (scale bar: 5μm).

1024 B) THP-1 derived macrophages were permeabilized using 0.5% TritonX-100 and
1025 stained with anti-Mannosidase-II antibody followed by the secondary antibody tagged
1026 with Alexa-560, fixed and visualized under the confocal microscope (scale bar: 5μm).

1027 C) THP-1 derived macrophages were nucleofected with mCherry-MAN2A. At 24
1028 hours post nucleofection, the cells were treated with Brefeldin A (20μM) for 4 hours
1029 and visualized under the microscope (scale bar: 5μm).

1030 D) U937 human macrophages, stably expressing the Golgi marker mRuby-
1031 B4GALT1 (red, β-galactosyl transferase). For the lower panel, B4GALT1 (red)
1032 expressing U937 macrophages were stained with anti-Mannosidase-II antibody
1033 followed by secondary antibody (Alexa-405, blue, scale bar: 5μm).

1034

Figure 2

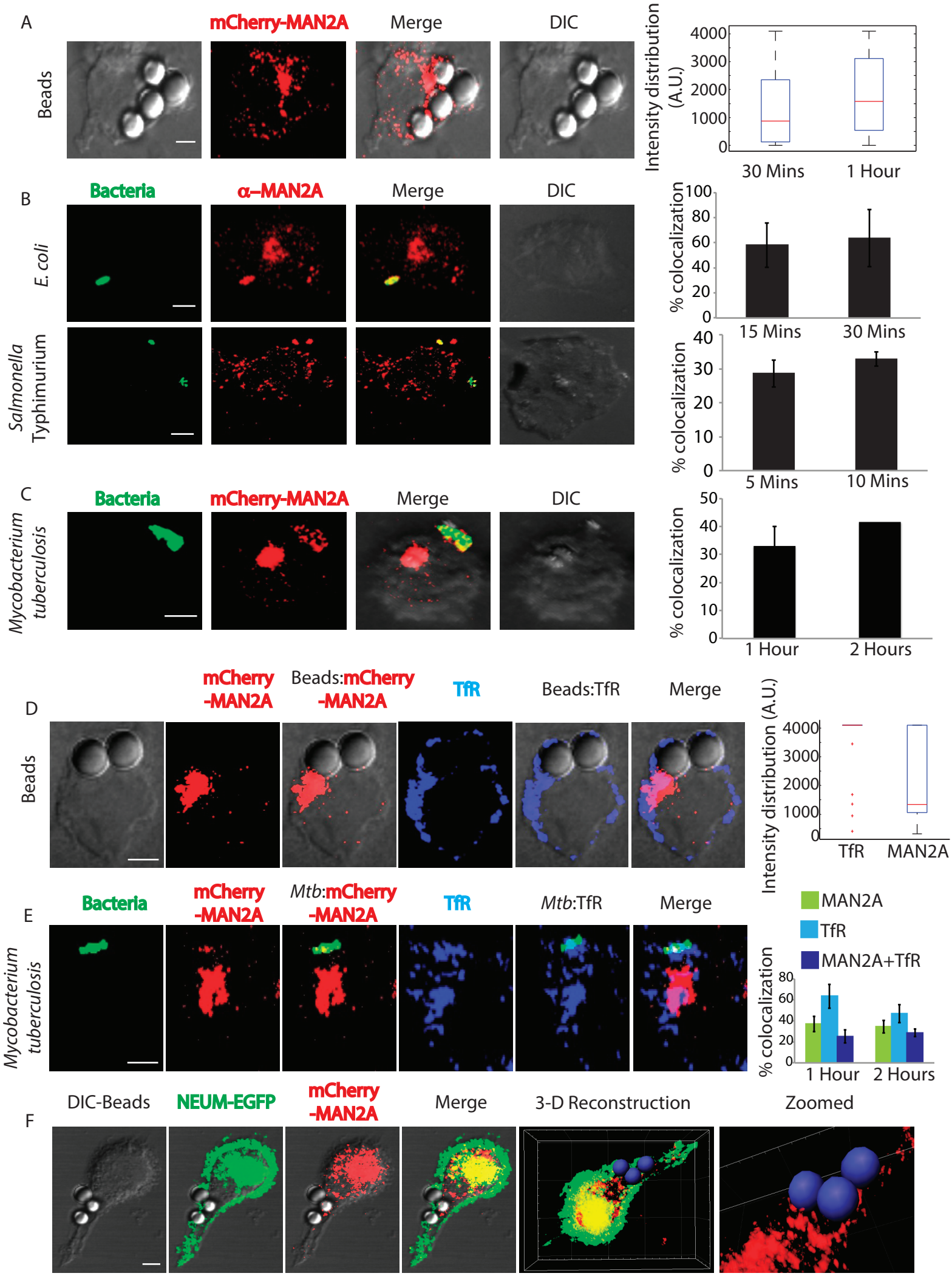
A
mCherry-MAN2A
Merge
DIC
Beads
Intensity distribution (A.U.)
4000
3000
2000
1000
0
30 Mins
1 Hour
B
Bacteria
α–MAN2A
Merge
DIC
E. coli
% colocalization
100
80
60
40
20
0
15 Mins
30 Mins
Salmonella Typhimurium
40
30
20
10
0
5 Mins
10 Mins
C
Bacteria
mCherry-MAN2A
Merge
DIC
Mycobacterium tuberculosis
50
40
30
20
10
0
1 Hour
2 Hours
D
mCherry -MAN2A
Beads:mCherry -MAN2A
TfR
Beads:TfR
Merge
Beads
Intensity distribution (A.U.)
4000
3000
2000
1000
0
TfR
MAN2A
E
Bacteria
mCherry -MAN2A
Mtb:mCherry -MAN2A
TfR
Mtb:TfR
Merge
Mycobacterium tuberculosis
MAN2A
TfR
MAN2A+TfR
% colocalization
80
60
40
20
0
1 Hour
2 Hours
F
DIC-Beads
NEUM-EGFP
mCherry -MAN2A
Merge
3-D Reconstruction
Zoomed

1035 **Figure 2: Mannosidase-II is recruited at the site of phagocytosis**

1036 A) RAW264.7 macrophages expressing mCherry-MAN2A (red) were incubated
1037 with mouse-IgG coated latex beads for 30 minutes and 1 hour. The images shown are
1038 representative from the 30 minutes samples. At the right, the total intensity of
1039 mCherry-MAN2A puncta on the bead surface was estimated using 3D spot creation
1040 module in Imaris 7.2 and the intensity distribution of the population has been plotted
1041 (see methods for detail). The box plot represents data from more than 200 beads
1042 analyzed from two different experiments (values ± S.D.; scale bar: 4μm).

1043 B) THP-1 derived macrophages were infected with PKH67 labeled *E. coli* (green,
1044 top panel) or GFP expressing *Salmonella* Typhimurium (green, lower panel) for 15
1045 and 30 minutes. Cells were then stained with anti-Mannosidase-II antibody followed
1046 by Alexa 568 tagged secondary antibody (red). Images shown are representative from
1047 the 15 minutes samples from both the experiments. The bar plots at the right show %
1048 co-localization of *E. coli* or *Salmonella* with Mannosidase-II at the surface at 5 and 10
1049 or 15 and 30 minutes respectively post-infection. Data represents average of more
1050 than 200 bacteria from two different experiments (values ± S.D.; scale bar: 3μm).

1051 C) mCherry-MAN2A (red) expressing THP-1 derived macrophages were infected
1052 with PKH67 labeled H37Rv (green) for 1 and 2 hours. Samples were fixed and
1053 visualized under the microscope. The bar-plot at the right shows % co-localization of
1054 H37Rv with Mannosidase-II at both these time points. Data represents average of
1055 more than 200 bacteria from two different experiments (values ± S.D.; scale bar:
1056 4μm).

1057 D) mCherry-MAN2A (red) expressing RAW264.7 macrophages were incubated
1058 with mouse-IgG coated latex beads for 30 minutes or 1 hour. At the respective time
1059 points, cells were immune-stained with anti-TfR antibody followed by a secondary

1060 antibody tagged with Alexa 405 (blue). Presence of TfR or Mannosidase-II at the
1061 bead surface was calculated in terms of fluorescence intensity using the 3D spot
1062 creation module in Imaris 7.2software. The box-plot at the right shows data from
1063 more than 100 beads from two independent experiments (scale bar: 5μm).
1064 E) mCherry-MAN2A (red) expressing RAW264.7 macrophages were infected
1065 with PKH67 labeled H37Rv (green) for 1 and 2 hours. At the respective time points,
1066 samples were fixed and stained with anti-Transferrin receptor antibody followed by
1067 Alexa-405 tagged secondary antibody (blue). The images are representative from the
1068 1 hour time point. For the plots at the right, % co-localization of H37Rv with
1069 Mannosidase-II, TfR or both Mannosidase-II and TfR was calculated using Imaris
1070 7.2. The data represents average of more than 150 bacteria from three different
1071 experiments (values ± S.D.; scale bar: 5μm).
1072 F) U937 cells stably expressing EGFP (green) at the plasma-membrane using a
1073 membrane targeting tag from Neuromodulin (NEUM-EGFP) were nucleofected with
1074 mCherry-MAN2A (red) and incubated with human-IgG coated latex beads for 30
1075 minutes. The 3-D constructions at the right hand side were performed using 3D spot
1076 creation module in Imaris 7.2 to visualize the juxtaposition of Mannosidase-II and
1077 latex beads against the plasma membrane (scale bar: 5μm).
1078

Figure 3

A

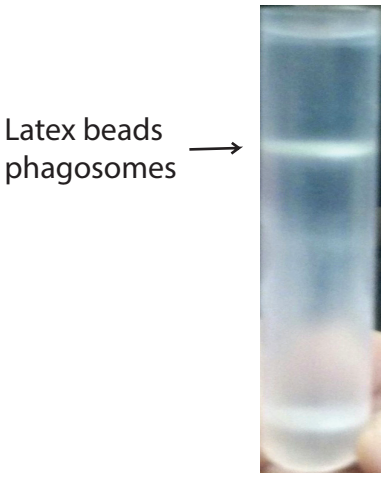
Latex beads
phagosomes

B

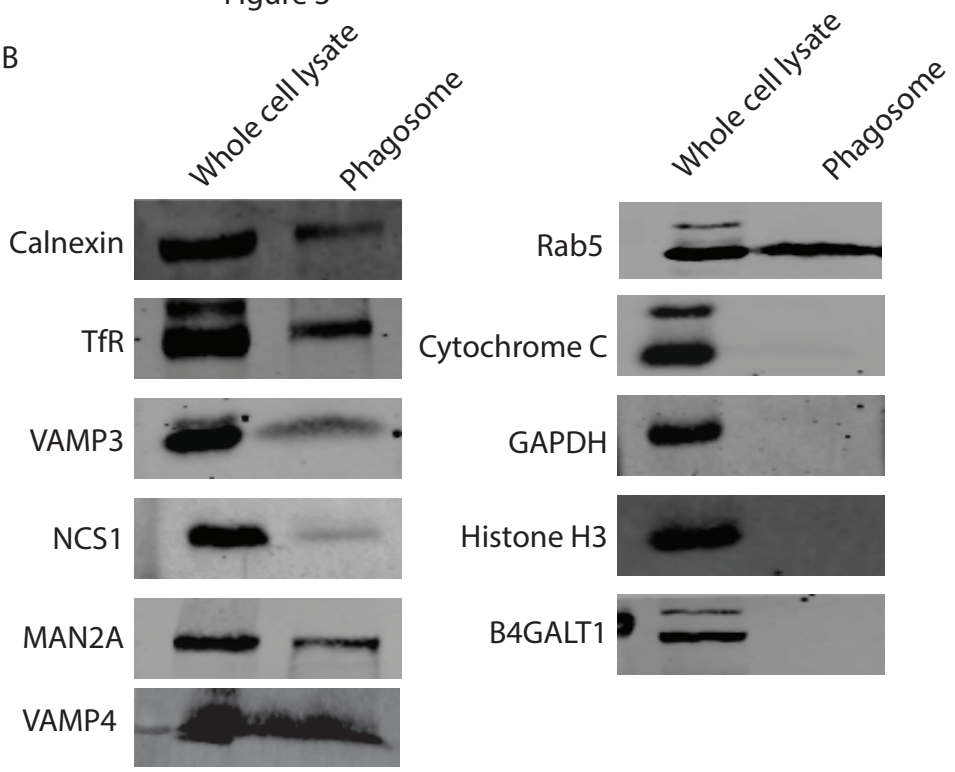
Whole cell lysate
Phagosome
Calnexin
TfR
VAMP3
NCS1
MAN2A
VAMP4
Whole cell lysate
Phagosome
Rab5
Cytochrome C
GAPDH
Histone H3
B4GALT1

C

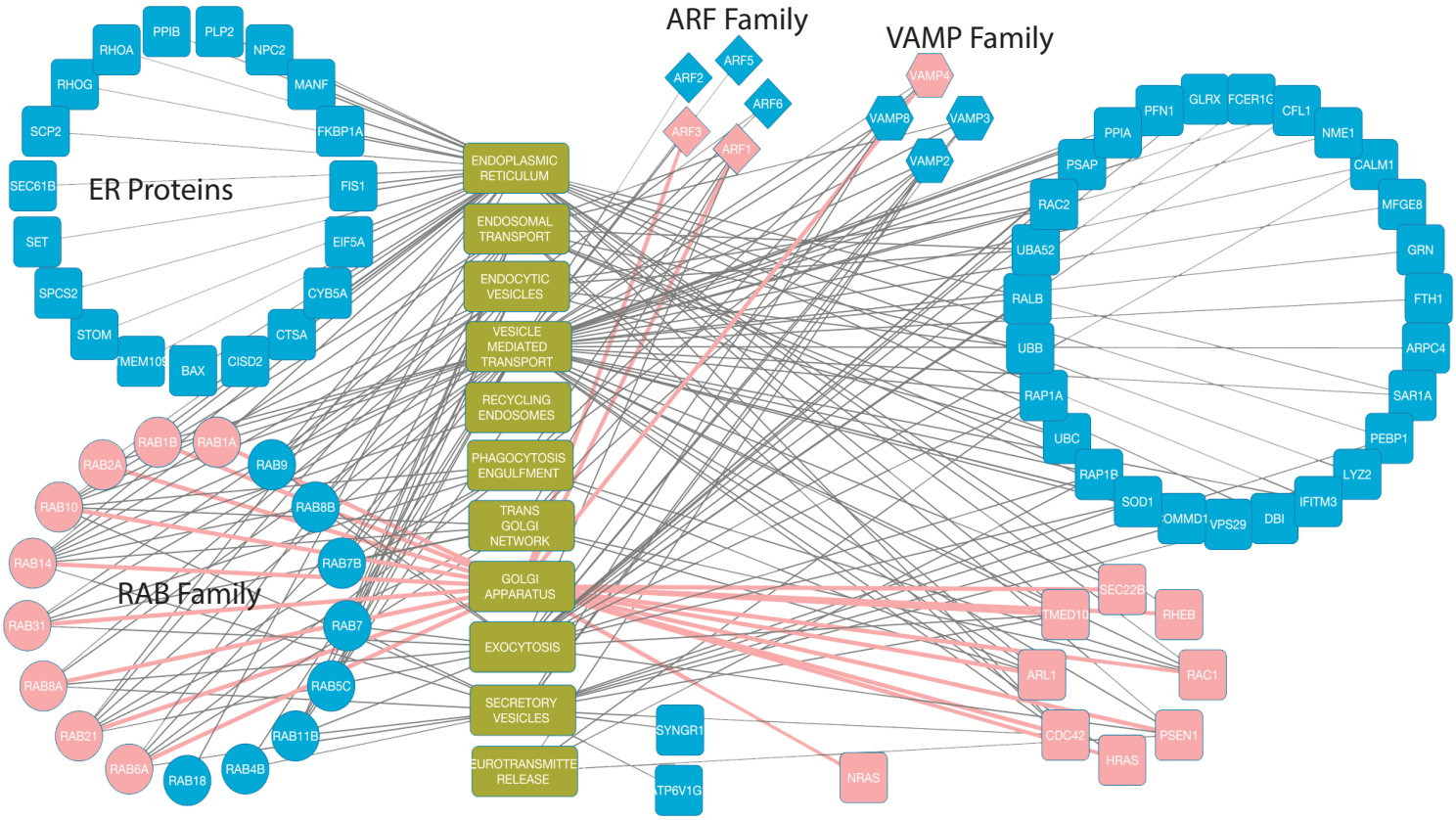
ER Proteins
RHOA
PPIB
PLP2
NPC2
RHOG
MANF
SCP2
FKBP1A
SEC61B
FIS1
SET
EIF5A
SPCS2
CYB5A
STOM
CTSA
MEM109
BAX
CISD2
ARF Family
ARF2
ARF5
ARF6
ARF3
ARF1
VAMP Family
VAMP4
VAMP8
VAMP3
VAMP2
ENDOPLASMIC RETICULUM
ENDOSOMAL TRANSPORT
ENDOCYTIC VESICLES
VESICLE MEDIATED TRANSPORT
RECYCLING ENDOSOMES
PHAGOCYTOSIS ENGULFMENT
TRANS GOLGI NETWORK
GOLGI APPARATUS
EXOCYTOSIS
SECRETORY VESICLES
EUROTRANSMITTE RELEASE
RAB Family
RAB1B
RAB1A
RAB2A
RAB9
RAB10
RAB8B
RAB14
RAB7B
RAB31
RAB7
RAB8A
RAB5C
RAB21
RAB11B
RAB6A
RAB18
RAB4B
PFN1
GLRX
FCER1G
CFL1
PPIA
NME1
PSAP
CALM1
RAC2
MFGE8
UBA52
GRN
RALB
FTH1
UBB
ARPC4
RAP1A
SAR1A
UBC
PEBP1
RAP1B
LYZ2
SOD1
IFITM3
COMMD1
VPS29
DBI
SEC22B
TMED10
RHEB
ARL1
RAC1
CDC42
PSEN1
HRAS
SYNGR1
ATP6V1G
NRAS

1079 **Figure 3: Proteomic analysis reveals presence of several VAMPs, ARFs and**
1080 **RABs in the early phagosomes**

1081 A) Preparation of latex bead phagosomes from THP-1 derived macrophages on a
1082 sucrose density gradient (see methods)

1083 B) THP-1 derived macrophages were incubated with latex beads (1μm size) for 1
1084 hour. Phagosomes were isolated using differential density ultracentrifugation and
1085 samples were probed for indicated markers using Western blots.

1086 C) Latex beads phagosomes isolated from RAW264.7 macrophages were lysed
1087 and resolved on a 10% SDS-PAGE (Fig. S2). The lane below 25kDa molecular
1088 weight was analyzed using mass spectrometry to identify enrichment of low
1089 molecular weight proteins (see methods). The list of genes identified was then
1090 searched in the AMIGO2.0 database to establish functional association. Finally the
1091 representative network was constructed using Cytoscape 2.6.1. The pink nodes and
1092 edges in the network denote association with the Golgi apparatus.

1093

Figure 4

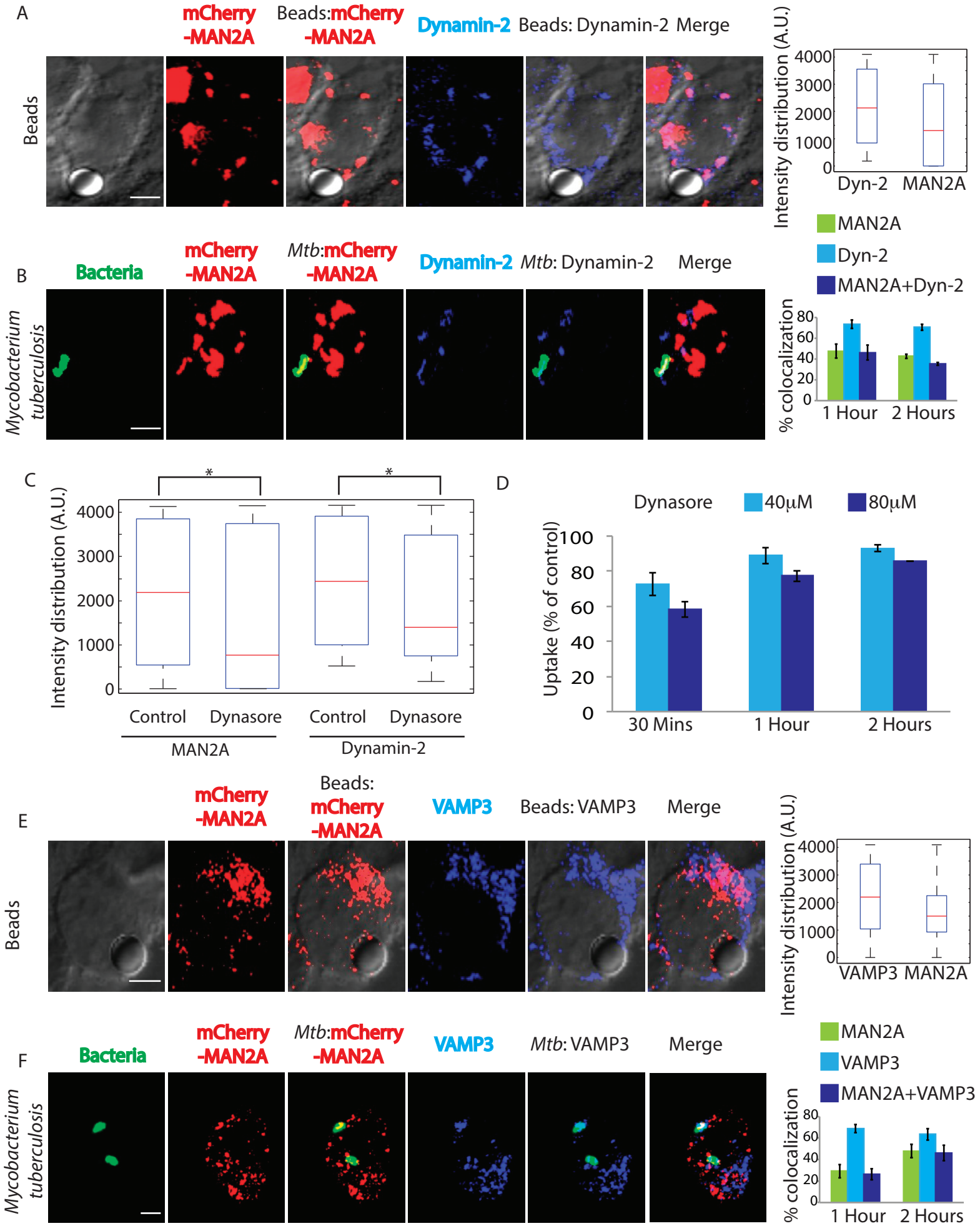
A
mCherry -MAN2A
Beads:mCherry -MAN2A
Dynamin-2
Beads: Dynamin-2
Merge
Beads
Intensity distribution (A.U.)
4000
3000
2000
1000
0
Dyn-2
MAN2A
MAN2A
Dyn-2
MAN2A+Dyn-2
B
Bacteria
mCherry -MAN2A
Mtb:mCherry -MAN2A
Dynamin-2
Mtb: Dynamin-2
Merge
Mycobacterium tuberculosis
% colocalization
80
60
40
20
0
1 Hour
2 Hours
C
*
*
Intensity distribution (A.U.)
4000
3000
2000
1000
0
Control
Dynasore
Control
Dynasore
MAN2A
Dynamin-2
D
Dynasore
40μM
80μM
Uptake (% of control)
100
80
60
40
20
0
30 Mins
1 Hour
2 Hours
E
mCherry -MAN2A
Beads: mCherry -MAN2A
VAMP3
Beads: VAMP3
Merge
Beads
Intensity distribution (A.U.)
4000
3000
2000
1000
0
VAMP3
MAN2A
F
Bacteria
mCherry -MAN2A
Mtb:mCherry -MAN2A
VAMP3
Mtb: VAMP3
Merge
Mycobacterium tuberculosis
MAN2A
VAMP3
MAN2A+VAMP3
% colocalization
80
60
40
20
0
1 Hour
2 Hours

1094 **Figure 4: Golgi-derived vesicles are recruited through focal exocytosis**

1095 A) mCherry-MAN2A (red) expressing RAW264.7 macrophages were incubated
1096 with mouse-IgG coated latex beads for 30 minutes or 1 hour. At the respective time
1097 points, cells were immune-stained with anti-dynamin2 antibody followed by a
1098 secondary antibody tagged with Alexa 405 (blue). Presence of dynamin2 (Dyn-2) or
1099 Mannosidase-II at the bead surface was calculated using the Imaris 7.2 software. The
1100 box-plot at the right shows data from more than 100 beads from two independent
1101 experiments (values ± S.D.; scale bar: 4μm).

1102 **B)** mCherry-MAN2A (red) expressing THP-1 macrophages were infected with
1103 PKH67 labeled H37Rv (green) for 1 and 2 hours. At the respective time points,
1104 samples were fixed and stained with anti-dynamin2 antibody followed by Alexa-405
1105 tagged secondary antibody (blue). The images are representative from the 1hour time
1106 point. For the plots at the right, % co-localization of H37Rv with Mannosidase-II,
1107 dynamin2 or both Mannosidase-II and dynamin2 was calculated using Imaris 7.2. The
1108 data represents average of more than 150 bacteria from three different experiments
1109 (values ± S.D.; scale bar: 4μm).

1110 C) mCherry-MAN2A (red) expressing RAW264.7 macrophages were pretreated with
1111 80μM Dynasore and incubated with mouse-IgG coated latex beads for 30 minutes or
1112 1 hour. At 30 minutes, samples were fixed and stained with anti-dynamin2 antibody
1113 followed by Alexa-405 tagged secondary antibody (blue). Intensity of Mannosidase-II
1114 and dynamin at the bead surface was calculated using the 3D spot creation module in
1115 Imaris 7.2 software. The box-plot shows data from more than 100 beads from two
1116 independent experiments (*p-value<0.05).

1117 D) THP 1 derived macrophages were treated with the respective dynasore
1118 concentrations for 4 hours and incubated with FITC labeled latex beads (1μm). At the

1119 respective time points cells were fixed and analyzed by flow cytometry. To calculate
1120 % uptake, data for each cargo for a given time point, the dynasore treated set was
1121 normalized against the respective untreated control set (values ± S.D.).
1122 E) mCherry-MAN2A (red) expressing RAW264.7 macrophages were incubated with
1123 mouse-IgG coated latex beads for 30 minutes or 1 hour. At the respective time points,
1124 cells were immune-stained with anti-VAMP-3 antibody followed by a secondary
1125 antibody tagged with Alexa 405 (blue). Presence of VAMP-3 or Mannosidase-II at
1126 the bead surface was calculated using the 3D spot creation module in Imaris 7.2
1127 software. The box-plot at the right shows data from more than 100 beads from two
1128 independent experiments (scale bar: 5μm).
1129 F) mCherry-MAN2A (red) expressing THP-1 derived macrophages were infected
1130 with PKH67 labeled H37Rv (green) for 1 and 2 hours. At the respective time points,
1131 samples were fixed and stained with anti-VAMP-3 antibody followed by Alexa-405
1132 tagged secondary antibody (blue). The images are representative from the 1hour time
1133 point. For the plots at the right, % co-localization of H37Rv with Mannosidase-II,
1134 VAMP-3 or both Mannosidase-II and VAMP-3 was calculated using Imaris 7.2. The
1135 data represents average of more than 150 bacteria from three different experiments
1136 (values ± S.D.; scale bar: 4μm).
1137

Figure 5

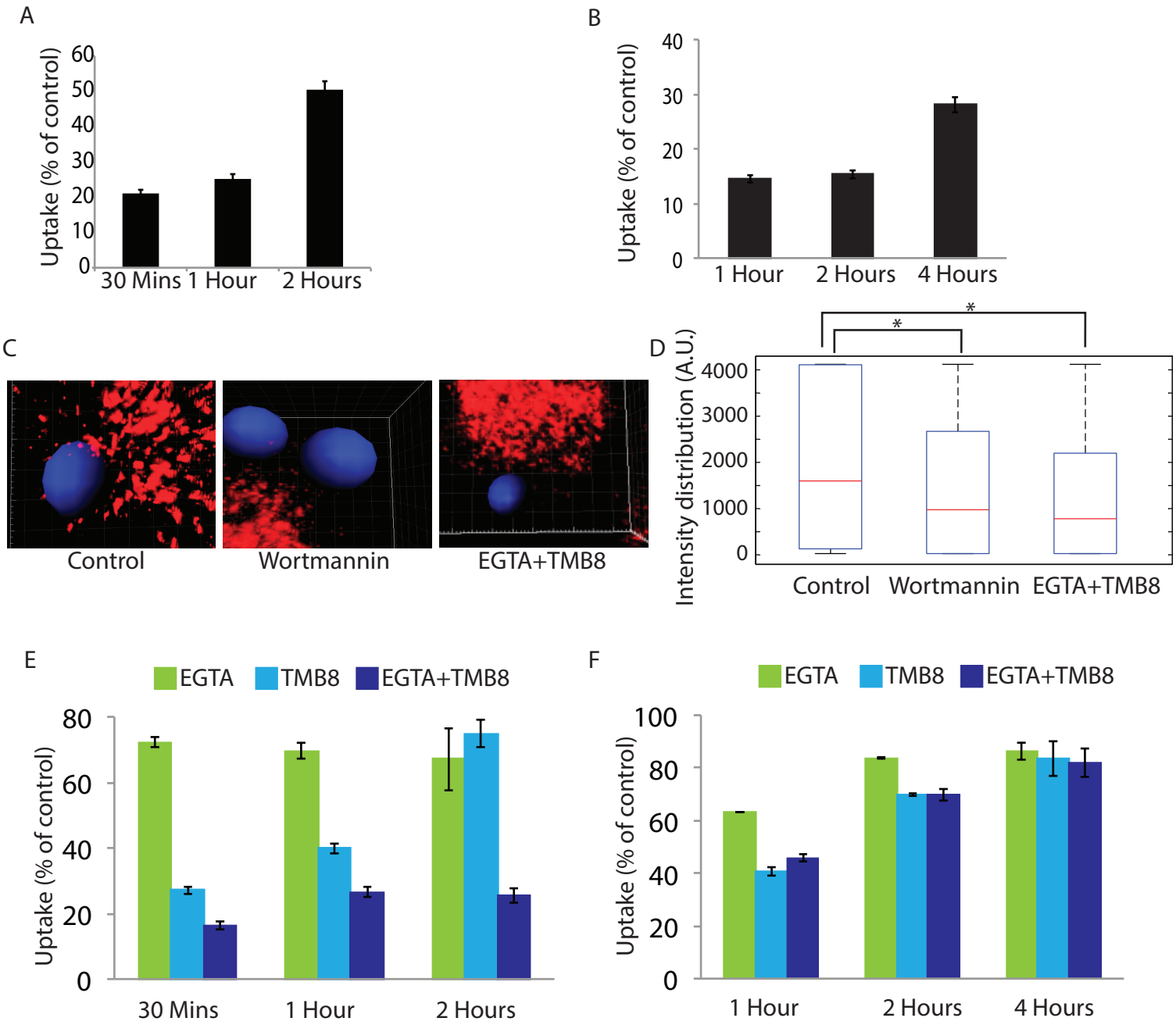
A
Uptake (% of control)
60
50
40
30
20
10
0
30 Mins
1 Hour
2 Hours
B
Uptake (% of control)
40
30
20
10
0
1 Hour
2 Hours
4 Hours
C
Control
Wortmannin
EGTA+TMB8
D
Intensity distribution (A.U.)
4000
3000
2000
1000
0
*
*
Control
Wortmannin
EGTA+TMB8
E
EGTA
TMB8
EGTA+TMB8
Uptake (% of control)
80
60
40
20
0
30 Mins
1 Hour
2 Hours
F
EGTA
TMB8
EGTA+TMB8
Uptake (% of control)
100
80
60
40
20
0
1 Hour
2 Hours
4 Hours

1138 **Figure 5: Role of PIP3 and Calcium from intra and extra-cellular sources in**
1139 **recruitment of Mannosidase II vesicles:**

1140 **A)** THP-1 derived macrophages were pre-treated with 5μM wortmannin for 4
1141 hours. FITC latex beads (1μm) were added to these. The cells were fixed at respective
1142 time points and analyzed by flow cytometry. Data shown are average from three
1143 different experiments and represented as % uptake in treated cells with respect to the
1144 untreated cells (values ± S.D.).

1145 B) THP-1 derived macrophages were pre-treated with 5μM wortmannin for 4
1146 hours. They were infected with PKH labeled H37Rv. At respective time points the
1147 cells were fixed and analyzed by flow cytomtery**.** Data shown are average from three
1148 different experiments and represented as % uptake in treated cells with respect to the
1149 untreated cells (values ± S.D.).

1150 C) mCherry-MAN2A (red) expressing RAW264.7 macrophages were pre-
1151 treated with 5μM Wortmannin or EGTA (3mM)+TMB8 (100 μM) for 30 minutes
1152 respectively. The cells were incubated with mouse-IgG coated latex beads for 30
1153 minutes or 1 hour. At the respective time points, cells were fixed and analyzed by
1154 confocal microscopy. The images shown are representative from the 30 minutes
1155 samples. The 3D construction of latex bead was done using spot creation module
1156 of Imaris 7.2.

1157 D) RAW264.7 macrophages expressing mCherry-MAN2A (red) were incubated
1158 with mouse-IgG coated latex beads for 30 minutes and 1 hour. The total intensity of
1159 mCherry-MAN2A puncta on the bead surface was determined using 3D spot creation
1160 module in Imaris 7.2 and the intensity distribution of the population has been plotted.
1161 The box plot represents data from more than 200 beads analyzed from two different
1162 experiments (*p-value<0.05).

1163 E) THP-1 derived macrophages were pre-treated with EGTA (3mM), TMB8
1164 (100μM) and EGTA+TMB8 for 30 minutes before addition of FITC latex beads
1165 (1μm). At respective time points the cells were fixed and analyzed by flow cytometry.
1166 Data shown are average from three different experiments and represented as % uptake
1167 in treated cells with respect to the untreated cells (values ± S.D.).
1168 F) THP-1 derived macrophages were pre-treated with EGTA (3mM), TMB8
1169 (100μM) and EGTA+TMB8 for 30 minutes before addition of PKH labeled H37Rv.
1170 At respective time points the cells were fixed and analyzed by flow cytometry. Data
1171 shown are average from three different experiments and represented as % uptake in
1172 treated cells with respect to the untreated cells (values ± S.D.).
1173

Figure 6

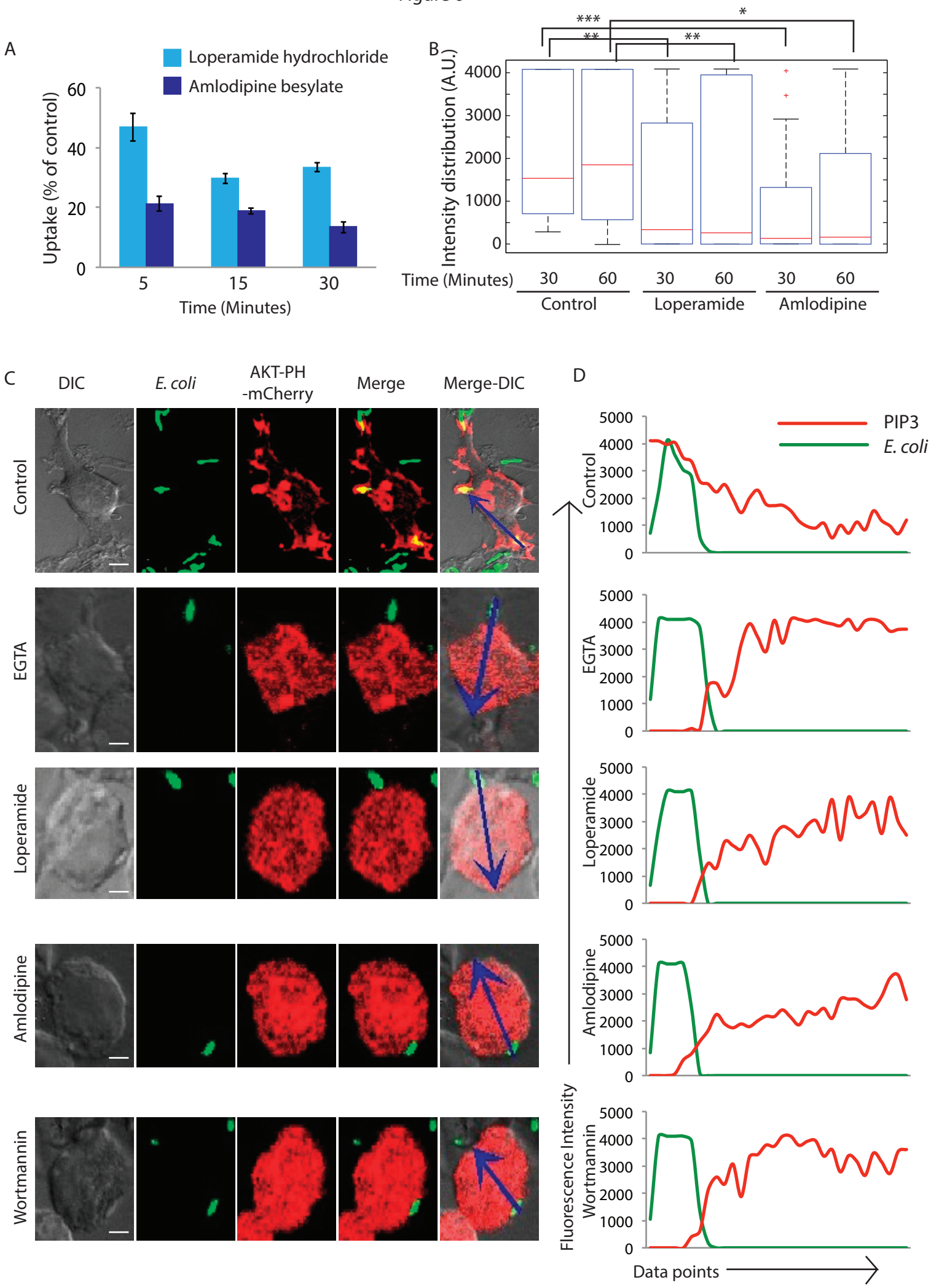
A
Loperamide hydrochloride
Amlodipine besylate
Uptake (% of control)
60
40
20
0
5
15
30
Time (Minutes)
B
***
**
*
**
Intensity distribution (A.U.)
4000
3000
2000
1000
0
Time (Minutes)
30
60
30
60
30
60
Control
Loperamide
Amlodipine
C
DIC
E. coli
AKT-PH -mCherry
Merge
Merge-DIC
Control
EGTA
Loperamide
Amlodipine
Wortmannin
D
PIP3
E. coli
Control
EGTA
Loperamide
Amlodipine
Wortmannin
5000
4000
3000
2000
1000
0
Fluorescence Intensity
Data points

1174 **Figure 6: Ca^{2+} entry through voltage-gated Ca^{2+} channel helps establish PIP3**
1175 **gradient to aid phagocytosis**

1176 **A)** THP-1 derived macrophages were pre-treated with Amlodipine (100µM) or
1177 Loperamide (100µM) for 30 minutes before addition of GFP expressing *E. coli*. At
1178 respective time points the cells were fixed and analyzed by flow cytometry**.** Data
1179 shown are average from three different experiments and represented as % uptake in
1180 the treated cells with respect to the untreated cells (values ± S.D.).

1181 **B)** RAW264.7 macrophages expressing mCherry-MAN2A (red) were pre-treated
1182 with amlodipine (100µM) or loperamide (100µM) for 30 minutes and subsequently
1183 incubated with mouse-IgG coated latex beads for 30 minutes and 1 hour. The total
1184 intensity of mCherry-MAN2A puncta on the bead surface was determined using 3D
1185 spot creation module in Imaris 7.2 and the intensity distribution of the population has
1186 been plotted. The box-plot represents data from more than 200 beads analyzed from
1187 two different experiments (*p-value<0.05, **p-value<0.01 and ***p-value<0.005).

1188 **C)** RAW264.7 macrophages were transfected with AKT-PH-mCherry. At 24
1189 hours of cells were incubated with GFP expressing E coli for 5 minutes. In parallel we
1190 also had AKT-PH-mCherry expressing cells that were pre-treated with EGTA (3mM),
1191 loperamide (100µM), amlodipine (100µM) or wortmannin (5uM) followed by
1192 incubation with GFP expressing *E. coli* for 5 minutes. Samples were fixed at 5
1193 minutes and analyzed by confocal microscopy. The arrows in the extreme right image
1194 in each of the panel highlight the fluorescence intensity measurements for the analysis
1195 presented in figure 6D (scale bar: 4µm).

1196 **D)** Images in figure 6C (arrows) were analyzed using intensity profile line tool in
1197 the NIS-elements software (see methods). The data represent median from more than
1198 20 fields for each case.

Figure 7

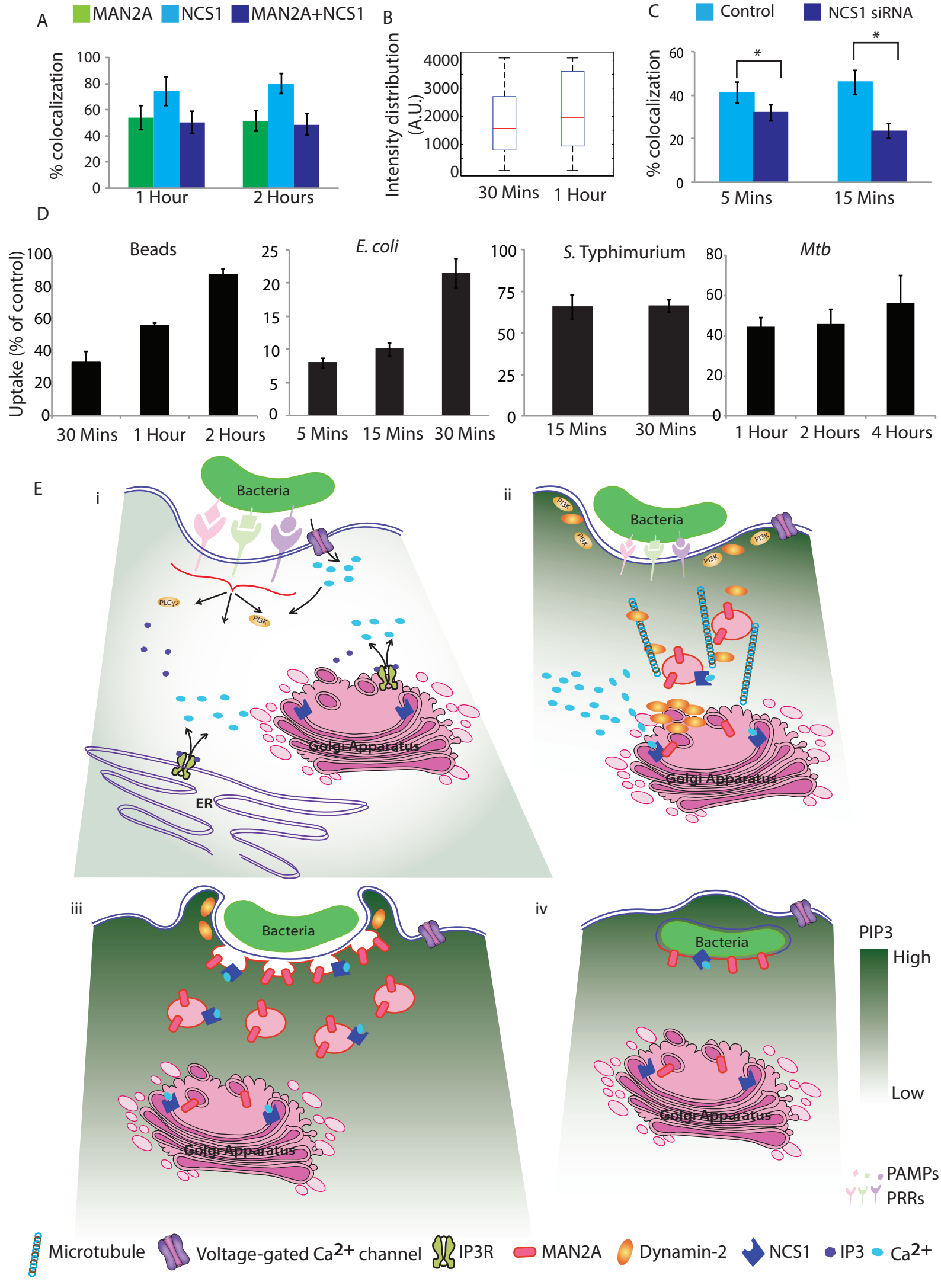
A
MAN2A
NCS1
MAN2A+NCS1
% colocalization
100
80
60
40
20
0
1 Hour
2 Hours
B
Intensity distribution (A.U.)
4000
3000
2000
1000
0
30 Mins
1 Hour
C
Control
NCS1 siRNA
% colocalization
60
40
20
0
*
*
5 Mins
15 Mins
D
Uptake (% of control)
Beads
100
80
60
40
20
0
30 Mins
1 Hour
2 Hours
E. coli
25
20
15
10
5
0
5 Mins
15 Mins
30 Mins
S. Typhimurium
100
75
50
25
0
15 Mins
30 Mins
Mtb
80
60
40
20
0
1 Hour
2 Hours
4 Hours
E
i
Bacteria
PLCγ2
PI3K
Golgi Apparatus
ER
ii
PI3K
Bacteria
Golgi Apparatus
iii
Bacteria
Golgi Apparatus
iv
Bacteria
Golgi Apparatus
PIP3
High
Low
PAMPs
PRRs
Microtubule
Voltage-gated Ca2+ channel
IP3R
MAN2A
Dynamin-2
NCS1
IP3
Ca2+

1199 **Figure 7: The neuronal calcium sensor (NCS1) in the Golgi apparatus recognizes**
1200 **Ca2+ signal for focal release of Mannosidase-II vesicles**

1201 A) mCherry-MAN2A (red) expressing U937 derived macrophages were infected
1202 with PKH67 labeled H37Rv (green) for 1 and 2 hours. At the respective time points,
1203 samples were fixed and stained with anti-NCS1 antibody followed by Alexa-405
1204 tagged secondary antibody. The images are representative from the 1hour time point.
1205 Percent co-localization of H37Rv with Mannosidase-II, NCS1 or both Mannosidase-II
1206 and NCS1 was calculated using Imaris 7.2. The data represents average of more than
1207 150 bacteria from three different experiments (values ± S.D.).

1208 B) In U937 macrophages, incubated with beads for 30 minutes or 1 hour, samples
1209 were stained with anti-NCS1 antibody. Presence of NCS1 at the bead surface was
1210 calculated using the 3D spot creation module in Imaris 7.2 software. The box-plot at
1211 the right shows data from more than 100 beads from two independent experiments.

1212 C) THP-1 derived macrophages treated with NCS1 siRNA were incubated with
1213 GFP expressing *E. coli* for 5 and 15 minutes. Cells were stained with anti-
1214 Mannosidase-II antibody to assess the recruitment of Mannosidase-II at the
1215 phagosomes in NCS1 depleted cells. The total intensity of mCherry-MAN2A puncta
1216 on the E coli surface was determined using 3D spot creation module in Imaris 7.2. For
1217 lower panel, percent co-localization of *E. coli* with Mannosidase-II was calculated
1218 using Imaris 7.2. The data represents average of more than 150 bacteria from three
1219 different experiments (values ± S.E.M, *p-value<0.05; scale bar: 2μm).

1220 D) THP-1 macrophages were treated with siRNA against NCS1 or scrambled
1221 control. At 48 hours post siRNA treatment, cells were monitored to uptake latex beads
1222 (1μm), *E coli*, *Salmonella* Typhimurium. or H37Rv for indicated time points. Data are
1223 shown as % uptake in the siRNA treated cells with respect to the scrambled siRNA

1224 control treated cells. Data are representative of three independent experiments (values
1225 ± S.D.).
1226 E) A model to explain the Ca2+ dependent activation of NCS1 to trigger the
1227 focal movement of Golgi derived vesicles. i) Initial recognition of an object (bacteria,
1228 beads, cell debris etc) for phagocytosis results in membrane depolarization possibly
1229 due to torsional stress and resulting in the activation of voltage gated Ca^{2+} channels,
1230 leading to the entry of extracellular Ca^{2+} into the cells. The entry of $Ca2^{+}$ through
1231 voltage-gated Ca^{2+} channels sets the focus for quick and efficient recruitment of PI3K
1232 and results in the accumulation of PIP3 at the site of phagocytosis. These early events
1233 are further aided by signaling through specific pattern recognition receptors and
1234 release of Ca^{2+} from intracellular stores. ii) Increased cytosolic Ca^{2+} is sensed by
1235 Golgi-resident NCS1, which triggers the movement of Mannosidase-II vesicles
1236 towards the site of phagocytosis, guided by a gradient of PIP3, along with dynamin
1237 and microtubule. iii) Mannosidase-II vesicles fuse with the membrane at the site of
1238 phagocytosis and help grow the phagosome around the cargo before final scission and
1239 internalization. iv) The membrane of the nascent phagosome is contributed in part by
1240 the plasma membrane and rest from the Golgi-derived vesicles (in this model for
1241 clarity, we have excluded lysosome and recycling endosomes as additional sources,
1242 see text).